



Parametric Study of Experimental and CFD Simulation Based Hydrodynamics and Mass Transfer of Rotating Packed Bed: A Review

Abdul Zahir¹ · Perumal Kumar¹ · Agus Saptoro¹ · Milinkumar Shah³ · Angnes Ngieng Tze Tiong¹ · Samreen Hameed²

Received: 15 December 2022 / Accepted: 19 April 2023
© The Author(s) 2023

Abstract

The emission of CO₂ into the atmosphere is one of the major causes of the greenhouse effect, which has a devastating effect on the environment and human health. Therefore, the reduction of CO₂ emission in high concentration is essential. The Rotating Packed Bed (RPB) reactor has gained a lot of attention in post-combustion CO₂ capture due to its excellent rate of mass transfer and capture efficiency. To better understand the mechanisms underlying the process and ensure optimal design of RPB for CO₂ absorption, elucidating its hydrodynamics is of paramount importance. Experimental investigations have been made in the past to study the hydrodynamics of RPB using advanced imaging and instrumental setups such as sensors and actuators. The employments of such instruments are still challenging due to the difficulties in their installation and placement in the RPB owing to the complex engineering design of the RPB. The hydrodynamics of the RPB can be affected by various operational parameters. However, all of them cannot be evaluated using a single instrumental setup. Therefore, the experimental setups generally result in a partial understanding of the flow behavior in the RPB. The cons and pros of experimental methods are reported and critically discussed in this paper. Computational Fluid Dynamics (CFD), on the other hand, is a powerful tool to visually understand the insights of the flow behavior in the RPB with accurate prediction. Moreover, the different multiphase and turbulence models employed to study the hydrodynamics of RPB have also been reviewed in-depth along with the advantages and disadvantages of each model. The models such as Sliding Mesh Model (SMM) and rotating reference frame model have been adopted for investigating the hydrodynamics of the RPB. The current research gaps and future research recommendations are also presented in this paper which can contribute to fill the existing gap for the CFD analysis of Rotating Packed Bed (RPB) for CO₂ absorption.

Abbreviations

RPB	Rotating packed bed
CFD	Computational fluid dynamics
SMM	Sliding mesh model
PCC	Post-combustion carbon capture
PIV	Particle image velocimetry
RTD	Residence time distribution
MRT	Mean residence time

E	Enhancement factor
MEA	Monoethanolamine
VOF	Volume of fluid
RSM	Reynolds stress model
DES	Detached Eddy simulation
MRF	Multi reference frame

Nomenclature

A	Gas–liquid interfacial area (m ² /m ³)
a _e	Effective interfacial area (m ² /m ³)
a _p	Surface area of the 2 mm diameter bead per unit volume of the bead (1/m)
a _t	Total area of the packing (m ² /m ³)
a _w	Wetted surface area of the packing, (m ² /m ³)
C _{AI}	Concentration of gas A at the gas–liquid interface on the liquid side (kJ/m ³)
C _{BL}	Concentration of liquid B in the bulk of the liquid (kJ/m ³)
C _t	Absorbent's total salt concentration, (g L ⁻¹)
D _A	Diffusivity of gas A (m ² /s)

✉ Perumal Kumar
p.kumar@curtin.edu.my

¹ Department of Chemical and Energy Engineering, Curtin University Malaysia, Sarawak, Malaysia

² Department of Chemical, Polymer & Composite Material Engineering, University of Engineering and Technology, New Campus, Lahore, Pakistan

³ Western Australia School of Mines: Mineral, Energy and Chemical Engineering, Curtin University, Bentley, WA 6102, Australia

D_{AL}	Diffusivity of CO ₂ in water A (m ² /s)	y_1	Mole fraction of CO ₂ in gas
D_L	Diffusion coefficient in the liquid phase (m ² /s)	y_2	Mole fraction of CO ₂ in outlet gas
d_h	Hydraulic diameter (m)	Y_k	Constant associated with the dissipation of k
d_p	Packing diameter (m)	Y_ω	Constant associated with the dissipation of ω ,
D_ω	Cross-diffusion constant.	Z	Packing height (m)
E	Enhancement factor of the gas–liquid flux due to the chemical	ϵ_L	Liquid Holdup
Fr	Froude number	ρ_l	Density of the liquid (g/m ³)
F_v	Volume force (N)	μ_L	Dynamic viscosity of the liquid (Pa s)
g	Gravitational acceleration (m/s ²)	σ	Surface tension (N/m)
G_a	Galilei number	γ	Contact angle (degree)
G_b	Generation of the turbulent kinetic energy due to buoyancy	ω	Angular velocity (rad/s)
G_k	Generation of the turbulent kinetic energy	α	Volume fraction
Gr	Grashof number	σ_ϵ	Prandtl numbers
G_1	Inert gas molar flow rate (kmol m ₂ h ⁻¹)	δ	Liquid side thickness (m)
H_d	Solubility coefficient (kmol/kpa m ³)	φ	Pore dimeter (m)
K_g	Gas side mass transfer coefficient (mol Pa ⁻¹ m ⁻² s ⁻¹)		
K_L	Liquid side mass transfer (m/s)		
K_1	Pseudo-first-order rate constant (s ⁻¹)		
k_2	Second-order rate constant of reaction (M ⁻¹ /s ⁻¹)		
L_m	Superficial mass velocity of the liquid (kg/m ² .hr)		
Q_L	Liquid flow rate (m ³ /s)		
ΔP	Pressure difference (Pa)		
ΔP_f	Pressure drop due to friction (Pa)		
ΔP_{ch}	Centrifugal pressure drop (Pa)		
ρ_L	Liquid density (Kg/l)		
ΔP_v	Pressure drop due to sudden change in volume (Pa)		
P_T	Total pressure (Pa)		
Q_G	Volumetric flow of the gas (L/min)		
R	Radial coordinate (m)		
R	Radial coordinate (m)		
R_A	Rate of absorption of A per unit volume (mol/m ³ s)		
Re	Reynolds number		
r_{in}	Inner radius of the packing (cm)		
r_{out}	Outer radius of the packing (cm)		
S	Stripping factor		
Sc	Schmidt number		
T	Temperature (K)		
U	Liquid Flow rate (m ³ /s)		
U_0	Characteristic flow rate per unit area (m ³ /s)		
V	Volume of the packing (m ³)		
u_o	Inlet velocity of the solvent (m/s)		
ν	Kinematic viscosity (Pa s)		
ν_o	Characteristic kinematic viscosity (Pa s)		
V_{liq}	Volume of liquid in packing (m ³)		
V_{total}	Total volume of packing (m ³)		
We	Weber number		
x_i	Mole fraction of solute in the inlet liquid stream		
x_o	Mole fraction of solute in the outlet liquid stream		

1 Introduction

Greenhouse gases have become a matter of serious concern in the twenty-first century because of the rapid increase in industrialization which demands a massive amount of power and energy. To meet those energy requirements, coal is widely used in the power sector. The huge consumption of coal for power generation produces greenhouse gases up to 46% worldwide and therefore is considered the single biggest contributor to the greenhouse gases [1]. There exist different CO₂ capturing approaches such as pre-combustion capture, oxyfuel and post-combustion carbon capture (PCC). Among these most widely adopted technologies, post-combustion carbon capture has gained a lot of attention due to its ease of application, low capital, and energy requirement [2]. Another most highlighted advantage of this technology is its ability to handle the high volume of CO₂ enriched gases and its retrofit nature; therefore, no radical change is required in the current industrial setup to adopt this technology [3]. Numerous techniques such as adsorption [4], membrane separation [5], cryogenics [6], absorption (Chemical and Physical), [7] and calcium looping carbon capture have been proposed and employed by the industries to reduce the emission of CO₂ to the atmosphere. Each of the remedial techniques has its limitations and disadvantages that outweigh its advantages. For example, adsorption is a useful technique as it does not discharge liquid waste effluent, however, it does not have a high adsorption capacity for CO₂ [8, 9]. Similarly, cryogenics is suitable for the CO₂ enriched gaseous stream, but its high energy consumption does not make it an economical choice [10]. Likewise, membrane separation is a simple and cost-effective technique, but the plasticization at high temperature and the trade-off between selectivity and permeability create barriers to its commercialization [11]. Therefore, among various proposed techniques, absorption has emerged as the most effective, mature and

reliable CO₂ capturing technique with promising capturing capacity [12]. Based on the type of attractive forces between CO₂ and the solvent, the absorption process can be classified into two categories, i.e., physical and chemical absorption. The favorable conditions for the physical absorption are the high pressure and low temperature, which require high energy consumption. This high consumption of energy to achieve those conditions results in an increase in the operational cost and thus makes the process uneconomical [13]. On the other hand, chemical absorption involves a chemical reaction between the solvent and the CO₂. The intermediate product formed as a result of chemical reaction, which binds the CO₂ with the solvent by forming a weak chemical bond. This weak bond can be dismantled to release the captured CO₂ when subjected to heat. Moreover, chemical absorption is more advantageous than the physical absorption due to its high absorption capacity and can handle gaseous streams having CO₂ partial pressure greater than 15% [14].

The selection of an appropriate solvent is a crucial factor that determines the feasibility as well as the efficiency of the absorption process. Based on the chemical and physical nature of absorption, the solvent can be categorized into chemical and physical solvents. Chemical solvents are those solvents that bind the CO₂ molecules by undergoing a chemical reaction with CO₂. The efficiency of the solvents can be predicted by their CO₂ absorption rate. As the reaction between solvent and CO₂ proceeds, the reduction of equilibrium partial pressure occurs, which increases the rate of absorption. One of the highlighted drawbacks of chemical solvents is the high energy consumption for the regeneration of solvent by breaking the bonding between the solvent and the CO₂ molecules [15, 16]. On the other hand, for physical solvents, the absorption of CO₂ is based on Henry's law, i.e., the amount of CO₂ dissolved in the solvent is proportional to the partial pressure of CO₂ above the solvent. The favorable condition to absorb the CO₂ is high pressure. Therefore, the desorption of gas can be done to regenerate the solvent by reducing the pressure [17].

The gas–liquid mass transfer majorly depends upon the configuration of the chemical reactor. Conventionally, packed bed reactors are being used for the chemical absorption of CO₂. This is the simplest configuration in which the CO₂-containing gases are passed through the fixed bed of the reactor. There are different packing structures available for this purpose. However, the major disadvantages inherent with this technology are the high capital, operational cost, high thermal efficiency penalty, low mass transfer rate and the use of concentrated amine-based solvent [18–21]. Lawal et al. [22] studied the post-combustion capturing of CO₂ through dynamic simulation and found that at least two packed columns were required with a minimum height up to 7 m and a diameter of 9 m each to achieve the capturing efficiency of CO₂ up to 90%. They concluded that this

specification of the column will lead to higher capital and operational cost and therefore, will increase the electricity cost by up to 50%. Riboldi and Bolland [23], while studying the performance of the packed bed reactor to capture CO₂ emitted from the coal power plant, found that the packed bed reactor imposes higher pressure drop even at a low gas flow rate; thus is not an effective absorber for the CO₂ absorption.

Alternatively, Rotating Packed Bed Reactor (RPB) is a process intensification device which was first introduced by HiGee Technology in 1990s. Rotating packed bed (RPB) has paved its way into various industrial processes such as separation and chemical reaction, distillation, stripping, absorption, production of nanoparticles, etc. The schematic diagram of a typical rotating packed bed is shown in Fig. 1 [24]. During the rotation of RPB, the rotor injects the liquid into the packing. The liquid passes through the packing of the RPB due to the shear force exerted on the liquid by the rotor and split into thin films and droplets which increases its surface area. This increase in the surface area, not only increases the mass transfer rate between the fluids but also reduces the reactor size and energy consumption [25, 26].

The conventional RPB consists of two major components, i.e., the rotor with the porous packing enclosed in a casing and the liquid distributor which inject and distribute the liquid homogeneously in the packing. The centrifugal acceleration produced by the rotor enhances the gas–liquid macromixing and provides better mass transfer between gas–liquid interface.

The RPB can be classified into different categories based on the following criteria.

- Phase contact type (counter-current, co-current, cross current).
- Number of rotor stages
- Type of the rotor
- Rotor orientation
- Type of packing

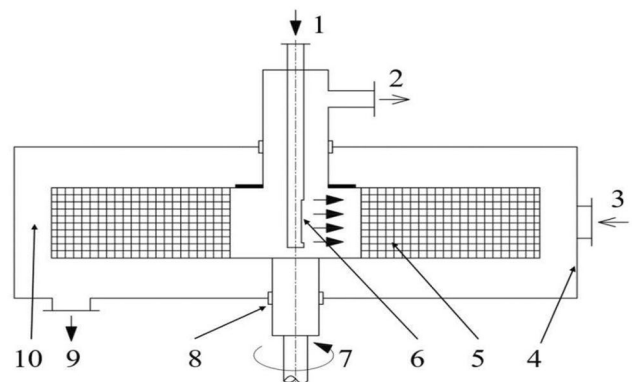


Fig. 1 Schematic diagram of RPB. 1. Liquid inlet, 2. Gas outlet, 3. Gas inlet, 4. Hull, 5. Packing, 6. Liquid distributor, 7. rotating shaft, 8. Seal, 9. Liquid outlet, 10. Cavity zone [27]

The selection criteria of RPB among the different types is based on the type of chemical process, the rate of mass transfer, liquid holdup, mean residence time, operational cost, pressure drop, ease of maintenance and the type of fluids [18, 28–30]. Furthermore, foam and wire mesh are being used conventionally as packing materials in RPB. The selection of packing material in RPB is based on the viscosity of the fluid. For the high viscosity fluids, wire mesh packing is more effective and provides better mass transfer rate as compared to the counterparts.

To the best of our knowledge, there exist very scarce data in the literature that critically highlights all the efforts made for the study of hydrodynamic parameters using experimental and empirical modelling. Moreover, the current scientific literature lacks to point out the pros and cons of the Computational Fluid Dynamics method to study the hydrodynamic parameters of the RPB, i.e., especially for the mass transfer performance of RPB. The previous studies do not completely address the critical aspects of the hydrodynamics of RPB in a single review such as the effect of different packing structures and RPB designs on the hydrodynamic parameters of the RPB, different approaches to estimate the mean residence time, advantages and disadvantages of different multiphase models, selection of suitable rotating reference frame model for different geometries and the reactive modeling of the CFD. This systematic review aims to critically analyze the experimental and CFD approach to study the hydrodynamics of the RPB. In the first section of the review, the hydrodynamic parameters such as liquid holdup, pressure drop, effective interfacial area, liquid residence time and mass transfer modelling by experimental methods in combination with the empirical modelling is reviewed critically. The later section focuses on the CFD studies, i.e., multiphase modelling of RPB, employment of turbulence models and the reactive modeling of CO₂ absorption.

2 Hydrodynamics of RPB

2.1 Experimental Studies

The hydrodynamic modeling provides useful information for all the changes that occur in the process with time. The rate of mass transfer is an important factor for the design and optimization of RPB for post-combustion CO₂ capture and depends on the hydrodynamics of the gaseous and liquid phases in RPB [27]. Hence, many researchers have tried to investigate the hydrodynamics of RPB by different non-invasive techniques such as high-speed photography and X-ray computed micro-tomography [31–33]. Yang et al. [32] used the X-ray Computed Tomography technique to study the hydrodynamics of CO₂ absorption in laboratory-scale RPB. The results were in the form of tomographic cross-sectional

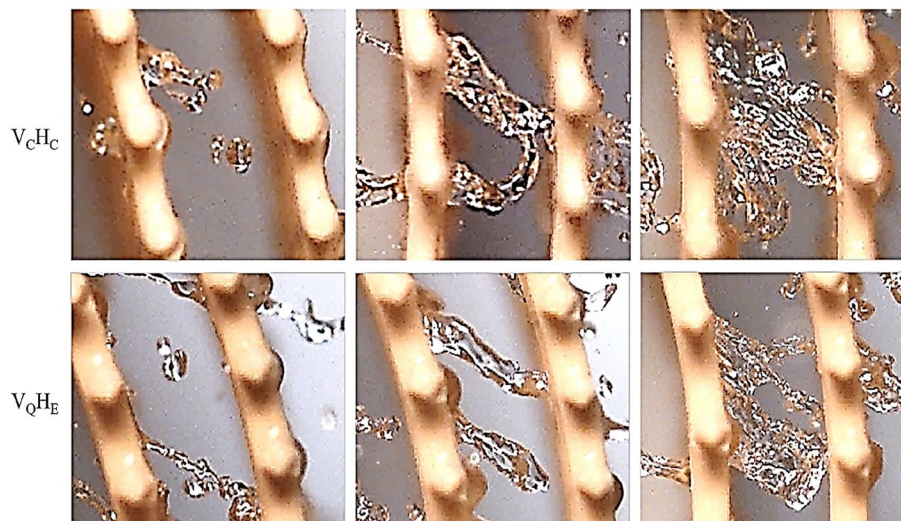
images and they found that the rotational speed and the solvent concentration had a considerable effect on the maldistribution of solvent around the packing region in RPB. The intensity of the X-ray was affected by the material of the reactor and was unable to provide any information regarding the flow characteristics of liquid films and liquid droplets. Yan et al. [34] studied the hydrodynamics of RPB by using colored water. The void cavities in the packing were filled with paper to investigate the liquid flow pattern of the colored water in RPB. This approach is cost-effective as it does not require any high-speed camera or the X-ray setup. However, this experimental setup can only capture the film flow within the RPB and no information regarding pore and droplet flow can be achieved using this technique. Likewise, Bongo et al. [35] employed the optical imaging technique by using Particle Image Velocimetry (PIV) to get the visuals of the velocity vectors of the liquid using the projections of the particles carried by the liquid. Burn et al. [36] used non-invasive techniques to study the hydrodynamics of absorption by investigating the fluid flow using a high-speed stroboscopic photography setup. The Wen et al. [37] used a high-speed camera to capture the film flow behavior in vertical quadrangular fibers and horizontal elliptical fibers (V_{QH_E}) and the packing composed of circular fibers (V_{CH_C}) in the RPB. The captured image exhibited the transition of liquid ligaments into droplets and liquid film as shown in Fig. 2. However, the non-invasive techniques were unable to provide detailed and accurate flow characteristics of the RPB and were expensive due to the special instrumental setup [34]. The experimental studies to investigate the hydrodynamics of the RPB are shown in Table 1.

2.2 Empirical Modeling of Hydrodynamic Parameters

2.2.1 Liquid Holdup

The liquid holdup in the RPB is the ratio of the volume of the packing zone to the volume of the liquid in the packing zone. This is an important hydrodynamic parameter that depicts the resilience of the packing zone to the liquid phase and is a crucial parameter for determining the mass transfer rate as well as the interfacial surface area. The value of the liquid holdup varies in each of the packing zone, i.e., the inner and outer zone has high liquid holdup while the bulk zone has comparatively low liquid holdup [39]. This critical variable primarily depends on various factors such as the inlet velocity of the liquid, solvent concentration, rotational speed and the contact angle of the packing. Yang et al. [32] and Grob et al. [40] used the advanced X-ray and Gamma-ray CT techniques, respectively, to determine the liquid holdup in the RPB. Both techniques have provided key information about the

Fig. 2 Liquid flow transition behavior in the RPB [37]



liquid holdup. However, the employment of these techniques is practically and economically not possible due to the expensive technical setup and the complex engineering design constraints in RPB. Therefore, various empirical models have been developed to calculate the liquid holdup in the RPB. However, all of these correlations are non-generic and, therefore, cannot be applied to all packing types and RPB configurations.

Burns et al. [41] placed an electrode in the packing of RPB and used the measurements of electrical resistance between the electrodes to develop the model for the prediction of liquid holdup in a highly porous packing. This model took into account the kinematic viscosity of the solvent and the rotational speed of the RPB. The experimental setup proposed by Burns et al. [41] is complicated and expensive as it requires the special set of equipment. Lin et al. [42] assumed that the liquid flow within the RPB is film flow and developed a correlation for the liquid holdup. The correlation is based on the measurement of the pressure drop and was relatively easy to calculate. Hendry et al. [43] used the empirical correlation (Eq. 1) to determine the liquid holdup in both the counter and co-current setup of the RPB. However, this is the simplest model and does not consider liquid–gas interaction in the RPB and thus, does not predict the accurate liquid holdup in the RPB.

$$\epsilon_L = 12.159\text{Re}^{0.923}\text{Ga}^{-0.61}\text{Ka}^{-0.019} \quad (1)$$

As the packing of the RPB is complex and the flow within the different zones cannot be assumed accurately, therefore, all the empirical correlations lag in their reliability and accuracy. Various proposed empirical correlations to determine the liquid holdup are summarized in Table 2.

2.2.2 Liquid Residence Time

Liquid residence time is an important aspect as it has significant effect on the mass transfer performance of the reactor and therefore affects the overall efficiency of the reactor. The liquid residence time can be optimized and can be employed for the scale up of the RPB [46]. The liquid residence time in the RPB can be measured by the Residence Time Distribution (RTD) data. Residence Time Distribution characterizes the ability of micro-mixing in the RPB and the study can be performed by monitoring the concentration of the tracer species at the outlet of the RPB over a certain period of time [47]. Guo et al. [46] used an experimental setup for the RTD study on the liquid flow in the RPB. The electrodes were placed on the rotor and the electrical pulse of the tracer species was monitored. They found that the operational parameters such as the liquid flow rate and the rotational speed of the RPB have considerable influence on the RTD. Likewise, Emami-Meibodi et al. [48] used the conductivity pen to detect the concentration of the tracer species at the outlet of the RPB and proposed a RTD model to calculate the liquid residence time. Their proposed model is as follows:

$$E(t) = \frac{1}{\tau} \quad (2)$$

$$\tau = \frac{V}{v} \quad (3)$$

however the model was based on the assumptions i.e., (i) volume of the pipes is so small that they can be neglected and (ii) there exists a solution gradient the feeding tank. The proposed model shows a good agreement with the experimental data with only a 2.5% difference. The mean residence time (MRT) of the RPB lies within the range of 0.4–1 s [46,

Table 1 Various experimental techniques used to study the hydrodynamics of RPB

RPB type	Packing type	Operating conditions	Technique	Limitations	Determinants	References
Counter-current	Wire Mesh Specific surface area: 498 1/m Void fraction: 0.95	Rotating speed: 500–2500 RPMs Liquid Flow rate: 1080–2580 mL/min	X-ray Computed Tomography	No information can be generated regarding the flow behavior, i.e., liquid film, droplet flow of the liquid.	Liquid holdup Mean Residence time	[32]
	Nickte foam Specific surface area: 1098 1/m Void fraction: 0.8					
Counter current flow	Annular packing Specific surface area: 1500 1/m Void fraction: 0.95	Rotating speed: 400–1200 RPMs Liquid Flow rate: 10.5 mL/min	Photoinaging camera, strobe light	Unable to provide visual evidence of film flow within the RPB.	Maldistribution of liquid	[36]
	Wire packing	Rotating speed: 500–1500 RPMs Liquid Flow rate: 400–1000 m ³ /hr	Sampling boxes around the packing	Following assumptions were made to determine the hydrodynamic parameters: The liquid flow on the packing is only the film flow. The liquid flow on the packing pores is only the droplet flow. Only one droplet forms during the liquid-wire impingement.	Liquid holdup	[38]
Co-current flow	Triangular spiral packing Specific surface area: 1500 1/m Void fraction: 0.95	Rotor speed: 450–1200 RPMs Liquid flow rate: 5–45 m ³ /h	Paper-dyeing technique	No information about the flow pattern can be extracted from this technique. Can only be used with hydrophilic packing materials. No information can be generated when the paper-liquid contact angle is greater than 90 due to the hydrophobic nature of the liquid.	Flow pattern/ Maldistribution of liquid	[34]
Co-current flow	Concentric wire mesh packing	Rotational speed: 400–2400 RPMs Liquid inlet velocity: 2.12–6.36 m/s	High speed camera	No useful information regarding gas holdup and pressure drop can be determined using this technique.	Flow behavior	[37]

Table 2 Correlations for liquid holdup estimation in RPB

Sr. no.	RPB configuration	Packing specification	Operating conditions	Liquid Holdup Correlation	References
1	Cross Flow	Blade packing Surface area: 1900 1/m Void Fraction: 0.89	Liquid velocity: 0.5–3.5 cm/s Rotor Speed: 200 m/s ²	$\epsilon_L = 0.039(\beta)^{-0.5} \left(\frac{U}{U_0}\right)^{0.6} \left(\frac{v}{v_0}\right)^{0.22}$	[44]
2	Cross flow	Surface area of the packing: 840 1/m Void Fraction: 0.954	Gas inlet velocity: 3.12–7.07 m/s Liquid velocity: 0.86–4.44 m/s Rotor Speed: 300–1500 RPMs	$\epsilon_L = 21.3u_{L,1}^{0.646}u_{G,2}^{-0.015}\omega^{-0.148}$	[45]
3	Counter-current Current–current	Metal mesh sheet Surface area of the packing: 663 1/m Void Fraction: 0.801	Solvent: Water Rotor speed: 500–2500 RPMs Liquid flow rate: 2580 mL/min	$\epsilon_L = 12.159Re^{0.923}Ga^{-0.61}Ka^{-0.019}$	[32]
4	Counter-current	Wire mesh packing Surface area of the packing: 497 1/m Void Fraction: 0.95	Liquid flow rate: 0.378 m ³ .h ⁻¹ Gas flow rate: 60 m ³ .h ⁻¹ Rotor Speed: 600 RPMs	$\epsilon_L = \frac{V_{liq}}{V_{total}} \times 100$	[40]
5	Counter-current	Glass beads	Liquid flow rate: 3.83 × 10 ⁻⁵ m ³ /s Gas flow rate: 150–1150 m ³ /s Rotor Speed: 91.11 rad/s	$\epsilon_L = \left[\frac{1}{r_o - r_i} \int_{r_i}^{r_o} h dr \right] a_w$	[42]

49, 50]. There are various factors other than the operational parameters which may affect the MRT such as the packing structure, RPB design, rate of the chemical reaction, phases interactions, packing wall adhesions, etc. Moreover, the optimum performance of RPB for the absorption of CO₂ can be achieved by adjusting the operational parameters, suitable selection of packing and the optimum RPB design [51].

2.2.3 Dry Pressure Drop

Dry pressure drop refers to the loss of gas pressure in the absence of liquid and, therefore, is an essential parameter to be considered to quantify the resistance offered by the packing and energy consumption to run the absorption process in RPB. To overcome the high-pressure drop, additional blowers and fans are required in the upstream, which increases the operational cost of the process [52]. Moreover, this parameter is also important to determine the parasitic load of the CO₂ absorption process and, thus, affects the feasibility of the absorption process in the RPB. The dry pressure drop in RPB is always higher than that of the packing bed reactor. But this can be compensated by the smaller reactor requirement due to its high mass transfer efficiency. In general, there are four zones in RPB that have significantly high-pressure drops as shown in Fig. 3

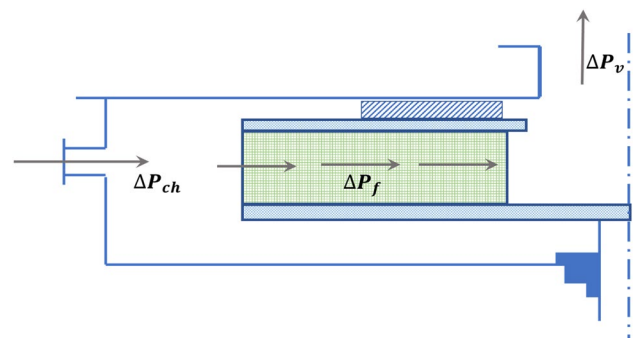
The main factors to contribute to the pressure drop are (i) the friction forces on gas molecules exerted by the packing and the solvent due to adhesion and the intermolecular forces between gas and the liquid, (ii) centrifugal head and (iii) increase in tangential velocity due to the change in area in the radial direction [53]. The total pressure drop, therefore, is the sum of pressure drop due to friction (ΔP_f),

centrifugal pressure (ΔP_{ch}) and the (ΔP_v), due to sudden change in the area.

Hendry et al. [43] calculated the pressure drop in RPB by the experimental setup and developed one-dimensional pressure drop model. However, the model cannot predict the pressure drop in all RPB's configurations. Likewise, Lin and Jian [54] studied the effect of operational parameters, i.e. liquid flow rate, gas flow rate and the rotor speed on the pressure drop and found that the pressure drop in the RPB increases with the increase in the gas flow rate and rotor speed but remains unchanged with the change in liquid flow rate. Moreover, they also developed empirical correlation for calculating the pressure drop in the RPB which is as follow

$$\Delta P = \frac{F_v^2}{2} \frac{a_t}{(\epsilon - h_L)^3} f_w (R_o - R_i) \quad (4)$$

Low pressure drop is favorable for any absorption process in the RPB. Optimum engineering design and selection of


Fig. 3 Zones for pressure drop in RPB

suitable packing material can help to achieve the low pressure drop in the RPB [55, 56]. Therefore, a detailed study of the pressure drop is important for the scale-up and the feasibility analysis of this process intensification technique for CO₂ absorption.

2.2.4 Effective Interfacial Surface Area

Interfacial surface area is the area of contact between gas and liquid and is the region where the mass transfer between the phases takes place. This important attribute is an essential prerequisite to determine the size of the RPB to achieve the desired rate of the mass transfer between the gas and the liquid [57]. The flow within the RPB is complex and is different from the conventional packed bed reactor. Therefore, various empirical and semi-empirical models have been proposed by the researchers. Im et al. [58] modified the correlation proposed by Billets and Schultes [59] by introducing the centrifugal acceleration in the correlation. Tsai and Chen [60] reported that the effective interfacial surface area can be increased up to 34% by using static baffles in the RPB. This increase in the effective interfacial area increases the overall mass transfer coefficient in the RPB. The correlations proposed for the calculation of RPB are summarized in Table 3.

2.3 Mass Transfer Modeling of CO₂ Absorption

Various experimental methods, in combination with the empirical correlations, have been employed to study the mass transfer performance of the RPB. The mass transfer between gas–liquid interface depends on various factors such as rotational speed (RPM), solvent concentration, contact angle, gas–liquid flow rates and the operational temperature [65]. The mass transfer mechanism inside the RPB is complex and therefore, no theoretical model can be developed to predict the mass transfer coefficient at any stage and zone of contact within the RPB. The volumetric gas and liquid side mass transfer coefficients are the two most important parameters while designing and optimizing the performance of RPB for the absorption process. Researchers have made various assumptions and developed different mass transfer models to predict the mass transfer coefficients at the gas–liquid interface.

Neumann et al. [66], due to the complex packing structure of the RPB, used the gas–liquid effective interfacial area as a considerable variable for the approximation of liquid side mass transfer in the RPB. The effective interfacial area was calculated using the expression below:

Table 3 Correlations for the interfacial surface area along with packing specifications

Sr. no.	Classification of RPB	Packing Specification	Interfacial area correlation	References
1	Counter current Flow	Packing type: Stainless steel	$a_c = \frac{R_A}{C_{A1} \sqrt{D_A} k_2 C_{BL}}$	[61]
2	Counter current Flow	Packing type: small mesh stainless steel Porosity (m ² /m ³): 0.76 Specific Surface Area (m ² /m ³): 213.2	$\frac{a_c}{a_p} = 1.5(a_p d_h)^{-0.5} \left(\frac{\rho_l u_l d_h}{\mu_L}\right)^{-0.2} \left(\frac{\rho_l u_l^2 d_h}{\sigma}\right)^{0.75} \left(\frac{u_l^2}{r \omega^2 d_h}\right)^{-0.45}$	[58]
3	Counter current Flow	Packing type: Raschig ring, Spherical rings, rods	$\frac{a_c}{a_i} = 1 - \exp\left(-1.45\left(\frac{\sigma_c}{\sigma_i}\right)^{0.75} \left(\frac{L_m}{a_i \mu_i}\right)^{0.1} \left(\frac{a_i L_m^2}{r \omega^2 \rho_i^2}\right)^{-0.05} \left(\frac{L_m^2}{\rho_i a_i \sigma_i}\right)^{0.2}\right)$	[62]
4	Counter current Flow	Packing type: Stainless steel Void fraction: 0.97 Specific Surface Area (m ² /m ³): 499.7	$a = \frac{A}{V}$	[57]
5	Two-stage counter current	Packing type: Nickle foam Void fraction: 0.956 Specific Surface Area (m ² /m ³): 342 Pore diameter: 5.08 mm	$a = \frac{A}{V}$	[63]
6	Counter Current	Packing type: Stainless steel wire mesh Void fraction: 0.94, 0.93, 0.94, 0.942 Specific Surface Area (m ² /m ³): 500, 450, 430, 385	$\frac{a_c}{a_p} = 66510 Re^{-1.41} We^{1.21} Fr^{-0.21} \varphi^{-0.74}$	[64]

$$a_{\text{eff}} = \frac{\Delta n_{\text{CO}_2, \text{Pack}}}{V_p C_{\text{I,CO}_2}^{\text{IP}} \sqrt{K_{\text{OH}^-} \cdot C_{\text{OH}^-} \cdot D_{\text{LCO}_2}}} \quad (5)$$

Likewise, Chen et al. [67] proposed the liquid side mass transfer correlation, which was valid for both Newtonian and non-Newtonian fluids. The correlation proposed by the Chen et al. [67] is as follows:

$$\frac{K_L a_{\text{d,p}}}{Da_t} \left(1 - 0.93 \frac{V_o}{V_i} - 1.13 \frac{V_i}{V_t} \right) = 0.65 Sc^{0.5} Re^{0.17} Gr^{0.3} We^{0.3} \quad (6)$$

Sun et al. [68] developed a mass transfer model to estimate the overall liquid side mass transfer coefficient for the simultaneous reactive absorption of CO_2 and NH_3 in the RPB. The predicted mass transfer coefficients were close to the experimental data and were within the bias range of 10%. Various proposed correlations to determine the mass transfer are summarized in Table 4.

2.3.1 Mass Transfer Modelling of Reactive CO_2 Absorption

The absorption of CO_2 into an appropriate solvent (such as MEA, K_2CO_3 , etc.) is a physio-chemical process. The absorption of CO_2 is considered physical if the absorption is based on Henry's law and the selectivity of CO_2 in a solvent occurs without any chemical reaction [81]. On the other hand, chemical absorption occurs as a result of the chemical reaction between solvent and CO_2 [82]. Enhancement factor (E) is a key parameter to predict the nature of absorption, i.e., chemical or physical. The E is the ratio of mass transfer rate due to the chemical reaction to the mass transfer rate without the chemical reaction. The absorption of CO_2 is considered as the physical absorption if the $E < 1$. Likewise, if the $E \geq 1$, the absorption is considered as the chemical absorption [83, 84].

Jasmine et al. [85] developed a mass transfer model (Eq. 8) to study the effect of chemical reaction on the mass transfer performance of the RPB using MEA as a solvent.

$$K_G a = \frac{k_{\text{app}}}{H_{\text{CO}_2-\text{MEA}}} \epsilon_L \quad (7)$$

The apparent pseudo-first-order reaction rate constant (k_{app}) and Henry's law constant ($H_{\text{CO}_2-\text{MEA}}$) were incorporated into the mass transfer model to predict the overall volumetric mass transfer coefficient. They found that the instantaneous reversible reaction affects the mass transfer rate and the predicted results were close to the experimental data. Yi et al. [86] developed a mass transfer model (Eq. 2.9) by considering the effect of reaction between diethanolamine (DEA) and K_2CO_3 .

$$k_L = D_L \left(\frac{\sqrt{\frac{k_1}{D_L}}}{\tanh\left(\left(\sqrt{\frac{k_1}{D_L}} \frac{d}{2}\right) - \frac{2}{D}\right)} \right) \quad (8)$$

$$k_1 = k_{\text{OH}^-} C_{\text{OH}^-} + k_{\text{DEA}} C_{\text{DEA}} \quad (9)$$

Based on this model and by comparing the calculated results with experimental data, they concluded that the mass transfer rate is much higher in the end zone region of the RPB as compared to the other regions.

The experimental method is an expensive and time-consuming approach. Furthermore, the results are also very difficult to be reproduced and thus, decrease the validity of the results. Similarly, data obtained by theoretical or analytical approach is not realistic as a lot of assumptions need to be made to simplify the mathematical models due to the complexity of the process. Therefore, the mass transfer rate, liquid holdup, effective interfacial area and pressure drop obtained by the theoretical or analytical methods do not cover all the parameters of consideration and, thus, cannot be used for the practical applications. For the semi-empirical method, there exists very limited data in the literature and cannot be used for determining the mass transfer rate due to lack of generalization in the mathematical models and their respective governing equations.

3 CFD Studies

CFD has proved itself as a cost-effective tool in modern-day engineering as it can solve complex fluid flow problems without compromising the accuracy and reproducibility. It has a promising potential to evaluate the hydrodynamic parameters and mass transfer rate by substantially declining the time and cost. Furthermore, CFD provides a detailed and graphical demonstration of data i.e., occurrence of flow separation or deviation of any set parameter from the maximum or minimum limit, which is not possible to achieve with the rest of the available techniques [87]. CFD analysis of the RPB can provide useful information about the hydrodynamic parameters such as liquid holdup, liquid residence time, pressure drop and liquid dispersion.

3.1 Effect of Operational Parameters on Hydrodynamics of RPB

The liquid holdup is one of the most important parameters to study the hydrodynamics of the RPB. The value of the liquid holdup (ϵ_l) determines the resistance offered by the packing to the liquid within the flow domain, the possibility of liquid to be flooded and the gas-liquid interfacial area [51]. Xie

Table 4 Mass transfer models reported for the RPB

Sr. no.	Absorbent	Absorbate	Assumptions	Boundary conditions	Mass transfer correlation	Mass transfer coefficient	References
1	Glycerol	O ₂	i. The packing is randomly oriented at a certain angle with respect to the horizontal surface. ii. All the solvent is trapped in the end zone of the RPB packing.	Liquid flow rate = 143 and 258 mL/min Rotating speed = 600–500 RPMs	$K_L \alpha = \frac{Q_L}{\pi(r_o^2 - r_i^2)z} \ln \left[\frac{(1 - \frac{1}{2}) \frac{x_o + 1}{x_o}}{(1 - \frac{1}{2})} \right]$	$K_L \alpha = 0.006 - 0.083 \text{ l/s}$ [69]	[69]
2	MEA	CO ₂	i. 99% CO ₂ is captured by the solvent in the packing layer. iii. Packing consists of wire mesh with concentric annuli. iv. Packing is assumed to be arranged in a layer-to-layer structure in the form of woven structure of annular wires. v. The wire mesh packing has horizontal and vertical alignment of fibers. vi. The thickness of the single fibers is as same as the thickness of the single packing layer.	Liquid velocity = 0.7–3.5 m/s Rotational speed = 1000 RPMs MEA concentration = 1–3.5 mol/L CO ₂ flow rate = 0.5–2.5 m ³ /h	$K_{L,d} = D_L \left(\frac{\sqrt{\frac{K_L}{D_L}}}{\tanh \left(\sqrt{\frac{K_L}{D_L}} \frac{z}{d} \right)} - \frac{2}{d} \right)$ $K_{L,f} = \sqrt{\frac{K_L}{D_L}} \text{Sech} \left(\sqrt{\frac{K_L}{D_L}} \delta \right) \sinh \left(\sqrt{\frac{K_L}{D_L}} \delta \right)$ $k_{GC} = \frac{D_G}{d} \left(2 + 0.552 \text{Re}^{0.5} \text{Sc}^{\frac{1}{3}} \right)$ $k_{GP} = 2a_1 D_G \text{Re}^{0.7} \text{Sc}^{\frac{1}{3}} (a_1 d_p)^{-2}$	$k_{GP} = 0.003 - 0.004 \text{ molPa}^{-1} \text{m}^{-3} \text{s}^{-1}$ $k_{GC} = 0.0004 - 0.0028 \text{ molPa}^{-1} \text{m}^{-3} \text{s}^{-1}$	[70]
3	MEA	CO ₂	N/A	Gas flow rate: 9–66 L/min Liquid Flow rate: 0.2–0.5 L/min Rotating speed: 500–1800	$K_G a = \frac{Q_G}{\pi(R_o^2 - R_i^2)} \ln \left[\frac{C_i}{C_o} \right]$	$K_G a = 0.18 - 31/s$	[71, 72]
4	DETA	CO ₂	N/A	Gas flow rate: 3.5 m ² /h DETA concentration: 3 mol/L CO ₂ loading: 0.41 mol/mol	$K_G a_y = \frac{G_1}{\pi \text{PH}(c_{out}^2 - c_{in}^2)} \ln \left[\frac{Y_{\text{CO}_2, \text{in}}(1 - Y_{\text{CO}_2, \text{out}})}{Y_{\text{CO}_2, \text{out}}(1 - Y_{\text{CO}_2, \text{in}})} \right]$ $+ \left[\frac{Y_{\text{CO}_2, \text{in}}}{1 - Y_{\text{CO}_2, \text{in}}} - \frac{Y_{\text{CO}_2, \text{out}}}{1 - Y_{\text{CO}_2, \text{out}}} \right]$	$K_G a_y = 4.5 - 6 \text{ kmol m}^{-3} \text{ kPa}^{-1} \text{ h}^{-1}$	[73]

Table 4 (continued)

Sr. no.	Absorbent	Assumptions	Boundary conditions	Mass transfer correlation	Mass transfer coefficient	References
5	NaOH	<p>CO₂ + N₂</p> <p>i. Only droplet flow is considered while developing the mass transfer model.</p> <p>ii. Liquid flow in form of liquid droplets at RPMs > 600.</p> <p>iii. Gas-liquid interfacial area is equal to the total area of liquid droplets and the blades.</p> <p>iv. Gas flow rate, temperature and viscosity have no considerable effect on the shape and flow pattern of the droplet.</p>	N/A	$K_{L,a_c} = \frac{\sum_{n=1}^3 \int_{r_{in}}^{r_{out}} (K_{L,a_c})_{rd} + \sum_{m=1}^2 \int_{r_{in}}^{r_{out}} (K_{L,a_c})_{rd} + \int_{r_1}^{r_2} r dr}{\int_{r_1}^{r_2} r dr}$	K _{L,a_c} = 3–42.5 1/s	[74]
6	Water	N/A	N/A	$\frac{K_{L,adb}}{D_{aL}} \left(1 - 0.93 \frac{V_a}{V_l} - 1.13 \frac{V_l}{V_g} \right) = 0.355 Sc^{0.5} Re^{0.17} Gr^{0.3} We^{0.3}$ $\left(\frac{a_L}{a_p} \right)^{0.5} \left(\frac{c_s}{c_w} \right)^{0.5}$	K _{L,a=0.004–2.5 1/s}	[67]
7	Water	<p>CO₂ + NH₃</p> <p>i. The gas-liquid interfacial area is comprised of surface area of the packing and liquid fragments (droplets).</p> <p>ii. The value of the pressure drop in RPB is very small and therefore, it can be neglected.</p> <p>iii. There is no micromixing in the packing region near the rotor.</p> <p>iv. The liquid in the RPB exhibits no back-mixing during the flow.</p>	<p>Gas flow rate = 1600–2700 L/h</p> <p>Solvent Flow rate = 50–600 L/h</p> <p>Rotating speed = 800–1500 RPMs</p>	$K_{L1} = D_{AL} \left[\sqrt{\frac{k_L}{D_{AL}}} / \tanh \left(\sqrt{\frac{k_L}{D_{AL}}} \frac{d}{2} \right) - \frac{2}{d} \right]$ $K_{L2} = D_{AL} \left[\sqrt{\frac{k_L}{D_{AL}}} \operatorname{sech} \left(\sqrt{\frac{k_L}{D_{AL}}} \delta \right) \sinh \left(\sqrt{\frac{k_L}{D_{AL}}} \delta \right) \right]$ $K_{g,a} = \frac{RTQ_G}{\pi Z (r_o^2 - r_i^2)} NTU = \frac{RTQ_G}{\pi Z (r_o^2 - r_i^2)} \ln \left(\frac{y_i}{y_o} \right)$	<p>K_{L1} = N/A</p> <p>K_{L2} = N/A</p> <p>K_{g,a} = 0.0148–0.0255 KmolPa⁻¹ m⁻³ s⁻¹</p>	[68]
8	NaOH	<p>CO₂</p> <p>i. Plug flow conditions are employed on both liquid and gas phases</p> <p>ii. The pressure drop is same at each point in the radial and axial directions</p> <p>iii. The flow of gas and liquid is a steady flow</p>	<p>Gas flow rate = 40–100 m³/h</p> <p>Solvent flow rate = 50–250 L/h</p>	$k_{L,a_c} = 0.003689 Re_G^{0.5449} We_L^{0.5476} Ga^{0.3428}$	k _{L,a_c} = 0.18–1.33 1/s	[75]

Table 4 (continued)

Sr. no.	Absorbent	Absorbate	Assumptions	Boundary conditions	Mass transfer correlation	Mass transfer coefficient	References
9	(NH ₄) ₂ SO ₃ + NH ₄ HSO ₃	SO ₂	i. The gas phase molar fraction at equilibrium is zero.	Gas flow rate: 75–160 m ² /h Solvent Flow rate: 300–400 L/h Rotating speed: 400–1400 RPMs	$k_g a = 0.08 Q_G^{-0.01} Q_L^{0.56} N^{0.36} pH^{0.57} C_t^{-0.76} C_{SO_2}^{-0.09}$	$k_g a = 0.65 - 1.2$ KmolPa ⁻¹ m ⁻³ s ⁻¹	[76]
10	(NH ₄) ₂ SO ₃ + NH ₄ HSO ₃	SO ₂	i. The gas phase molar fraction at equilibrium is zero.	Gas flow rate: 75–160 m ² /h Solvent Flow rate: 300–400 L/h Rotating speed: 400–1400 RPMs	$K_{y1} a = 2.6 \times 10^{-4} Re_G^{0.60} Fr_G^{0.34} Ga^{0.47}$ $K_{y2} a = 6.7 \times 10^{-5} Re_G^{0.77} Fr_G^{0.21} Ga^{0.26}$	$K_{y1} a = 3.15 - 7$ 1/s $K_{y2} a = 3.6 - 6.5$ 1/s	[77]
12	Water	VOC	N/A	Liquid flow rate = 310–1030 mL/min Rotating speed: 500–1800 RPMs	$\frac{K_L a_{CL} d_p}{D_{a1}} \left(1 - 0.93 \frac{v_a}{v_l} - 1.13 \frac{v_l}{v_t} \right)$ $= 0.355 Sc_L^{0.5} Re_L^{0.17} Gr_L^{0.3} We_L^{0.3} \left(\frac{d_t}{a_p} \right)^{-0.5} \left(\frac{\delta_w}{\delta_w} \right)^{0.14}$	$K_L a_{CL} = 0.5 - 2.9$ 1/s	[78]
13	MEA	CO ₂	N/A	N/A	$\frac{K_L d_p}{D_L} \left(\frac{d_t}{a} \right)^{0.33} Sc_L^{0.5} Re_L^{0.2} Gr_L^{\frac{1}{6}}$	N/A	[79]
14	H ₂ O ₂	SO ₂	i. The flow of the hydrogen peroxide in the packing region is the film flow when the rotational speed is within the range of 200–800 rpm. ii. The flow of the hydrogen peroxide is the droplet flow when the rotational speed is within the range of 1000–1400 rpm. iii. The value of the pressure drop is negligible while developing the mass transfer model. iv. There is no volatilization of the hydrogen peroxide during the absorption process. v. The absorption process is isothermal.	N/A	$K_L = D_{SO_2} \left(\frac{\sqrt{\frac{k_{SO_2}}{b_{SO_2}}}}{\tanh \left(\sqrt{\frac{k_{SO_2} d}{b_{SO_2} \tau} - d} \right)} \right)$ $\frac{K_G Re_G^T}{a_{D,G}} = 2 Re_G^{0.7} Sc_G^{0.33} (a_t d_p)^{-2}$	N/A	[80]

et al. [27] investigated the liquid holdup of 50 wt% MEA solution by varying the operational conditions such as the rotational speed, inlet velocity and MEA concentration and found that the rotational speed has a significant effect on the liquid holdup performance of RPB. At higher rotational speed, the MEA ligaments were transformed to tiny droplets and were not under the influence of any resistance offered by the packing. Therefore, the residence time of MEA in the RPB decreased up to 70% when the rotational speed was increased to 1500 rpm, thus also decreased the liquid holdup of MEA. There are various operational parameters that can influence the liquid holdup in the RPB such as the inlet velocity, solvent concentration and packing-solvent contact angle. However, among these parameters, the inlet velocity has a minor effect on the liquid holdup in the RPB [27]. Xie et al. [27] also reported that the concentration of the MEA has a noticeable effect on the liquid holdup as with the increase in concentration, the dynamic viscosity increases considerably. This increase in viscosity improves the adhesion of the solvent with the packing surface, which increases the residence time and the liquid holdup. Similarly, Zhang et al. [88] reported that hydrophobic packings at the entrance of the packing can reduce the liquid holdup up to an optimum level which can avoid the possible flooding of the solvent at the inlet location. They also concluded, as a result of the 3D CFD simulation of RPB, that at low rotational speed, the packing offers noticeable resistance for the incoming liquid and, thus, exhibits high residence time. The effect of different rotational speeds on the liquid holdup can be seen in Fig. 4 and the equations to calculate the mean residence time are summarized in Table 5.

Shi et al. [89] used the Residence Time Distribution (RTD) method to calculate the MRT. After the achievement of pseudo-steady state, a tracer with the same physical properties as of the water was injected into the RPB through the inlet with the volume fraction of 1 for a very short instance of time, i.e., 0.01 s. The volume fraction of the tracer at the outlet was then monitored continuously to get the RTD curve. Likewise, Burn et al. [41] calculated the mean residence time as a function of the liquid holdup. The liquid holdup was determined by installing the resistance measuring detectors to measure the liquid holdup resistance in the RPB. The value of the liquid holdup was then used in Eq. 1 of Table 5.

The mass transfer within the RPB depends on how long the gas and liquid come in contact with each other and, therefore, is very crucial in determining the potential of RPB for the CO₂ absorption. To achieve an optimum residence time, the gas flow rate is used to tune the gas residence time whereas, the liquid residence time can be tuned by various operational parameters such as the liquid velocity, rotational speed and nature of the packing [92]. Yang et al. [93] studied the liquid residence time by varying the center

distance between the packing layers (Δd) and found that by decreasing the center distance, the liquid residence time increases due to an increase in its surface area which eventually enhances the mass transfer between the gas-liquid phase. This increase in the mass transfer is advantageous to achieve high removal capacity. The effect of the packing structure on the residence time can be seen in Fig. 5.

Whang et al. [94] studied the effect of droplet velocity on the average residence time of the liquid in the RPB and found that change in the rotational speed and liquid inlet velocity can alter the mean residence time of the liquid, as shown in the Fig. 6.

Malinowska et al. [95] studied the pressure drop as a function of rotational speed in the porous packing in the RPB using a 3D CFD model. The CFD results of two turbulence model, i.e. RNG $k - \epsilon$ and Standard $k - \epsilon$ were compared with the experimental data. The CFD results started to deviate from the experimental data with the increase in the gas flow rate. However, the discrepancy was less than 20%, which lies within the acceptable limits of error.

3.2 Effect of Packing Structure on the Hydrodynamics of RPB

The type of the packing structure has a considerable effect on the hydrodynamics and mass transfer efficiency of RPB and is, therefore, considered a key parameter to evaluate the efficiency of RPBs. These packing in general can be categorized as wire mesh and foam packing. The wire mesh structure is subcategorized as structured, unstructured, weaved meshed, knitted meshed and zigzag wire mesh packings. Different packing structures of RPB are shown in Fig. 7. Based on the mass transfer coefficient, wire mesh packing offers more promising performance as compared to its counterparts [67]. Qammar et al. [96] compared the mass transfer efficiency and hydrodynamics of different wire mesh packings by experimental study and found that zigzag wire mesh structure exhibited the highest mass transfer as compared to the conventional wire mesh packing. This packing structure also offers low-pressure drop, which decreases the operational cost and makes the process more economical. The advantages and disadvantages of different RPB packing structures are summarized in Table 6.

Moreover, due to the complex packing structure of the RPB, it is difficult to develop an exact packing geometry for the CFD study. Therefore, a lot of simplifications and assumptions are required to be made to develop a simplified structured geometry. Due to these assumptions, accurate prediction of the fluid flow behavior around the packing material cannot be obtained by the CFD study [98]. Square wire mesh packing and circular wire mesh packings are the most widely used geometries for the hydrodynamic study of RPB by CFD. Due to the short computational time and ease

Fig. 4 Effect of different operational conditions on the liquid holdup [90, 91]

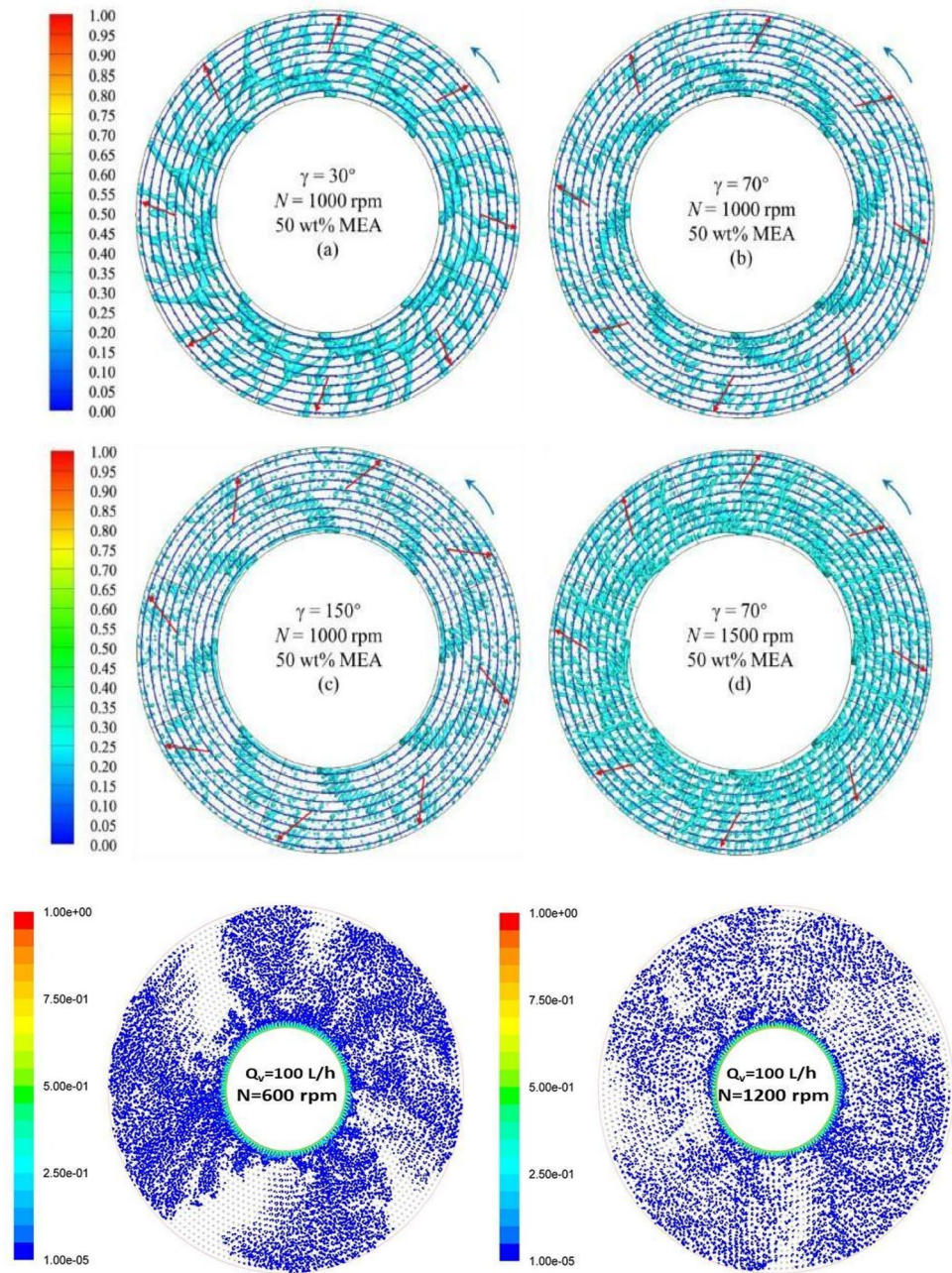


Table 5 Equations for Liquid residence time in RPB

No.	Equation	Description	Proposed by
1	$t \approx \frac{\epsilon_1}{U} (r_o - r_1)$ $U = \frac{u_0 d}{2\pi r}$ $r = \frac{(r_o + r_1)}{2}$	ϵ_1 = liquid holdup of the liquid U = superficial liquid velocity r_o = inner radius of the packing r_1 = outer radius of the packing d = width of the injection nozzle	Burns et al. [41]
2	$t = \frac{\sum t_i F_i}{\sum F_i}$	F_i = volume fraction of tracer at the outlet at time t_i	Shi et al. [89]

of geometry development, 2D geometric models have been employed extensively for the CFD analysis of RPB [50, 89, 93, 98, 102-106]. The different 2D geometry designs of RPB are shown in Fig. 8.

However, the prediction of the hydrodynamic parameters such as liquid holdup, residence time and maldistribution with the 2D model is not as accurate as the 3D model. Therefore, various studies have been done so far using the 3D CFD models. Goa et al. [103] used the 3D model to study different characteristics of liquid flow behavior, such as maldistribution of liquid, mean residence time and specific surface area and concluded that the simulated results showed a better agreement

Fig. 5 Effect of packing structure on the residence time: **a** $\Delta d=3$ mm; **b** $\Delta d=2.5$ mm [91]

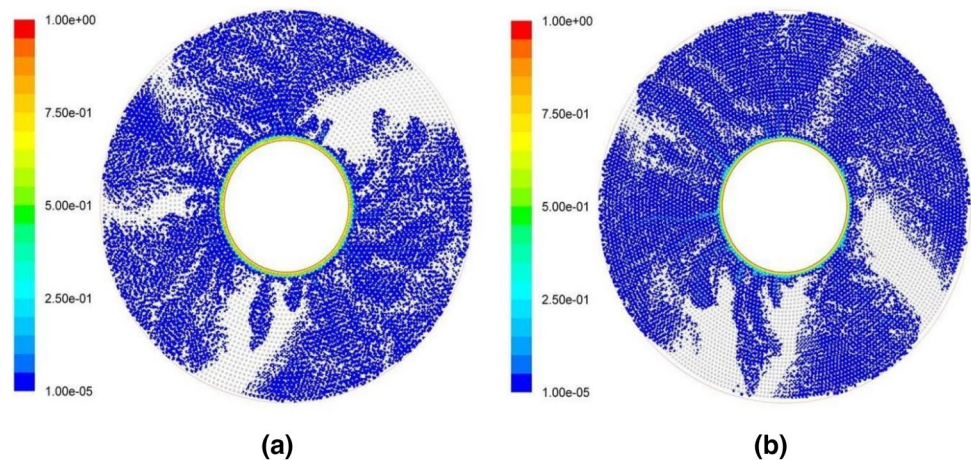
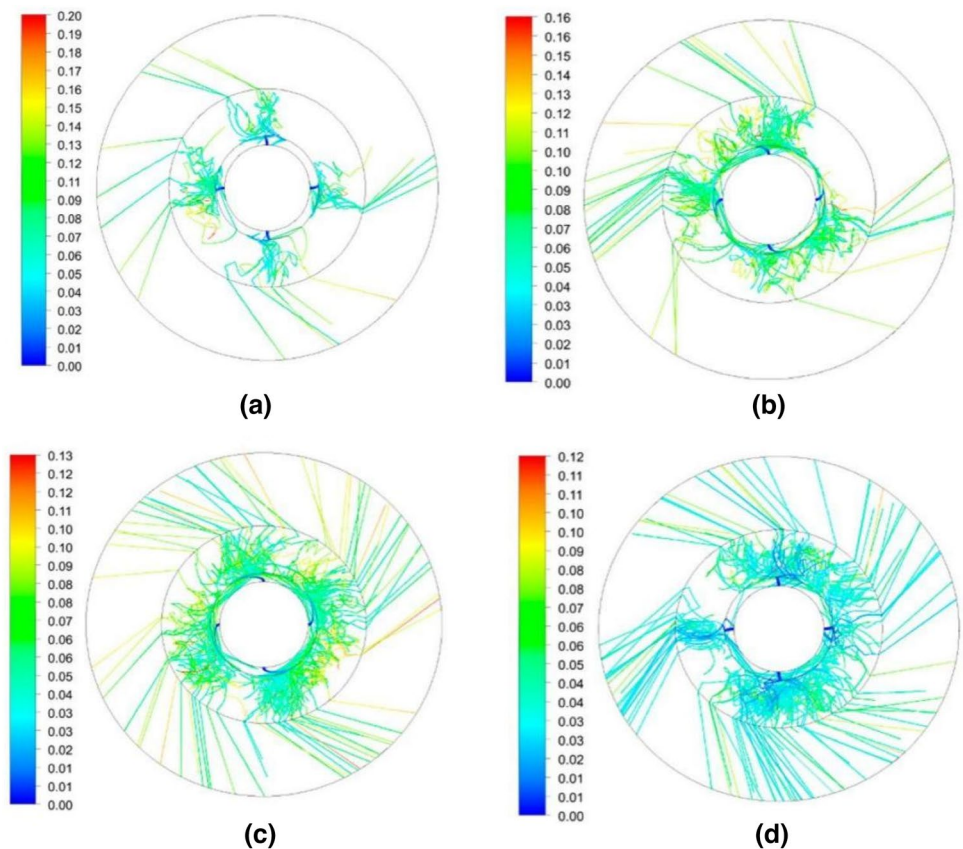


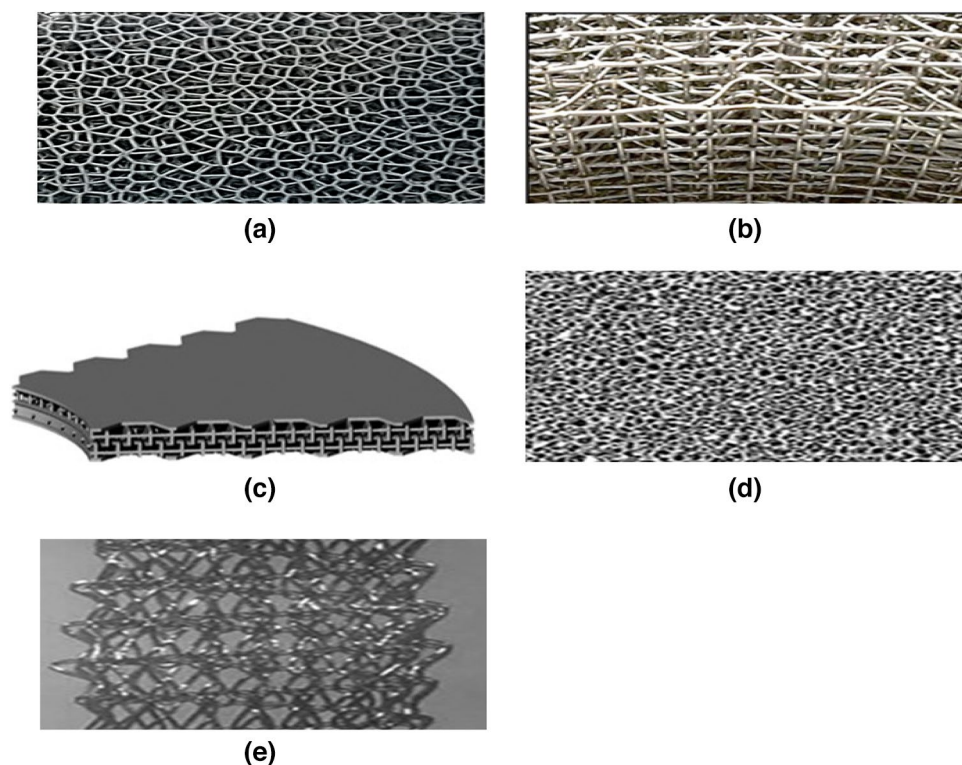
Fig. 6 Residence time distribution in RPB at different droplet velocities and rotational speeds. **a** $u_0=0.5$ m/s, $N=300$ rpm; **b** $u_0=0.5$ m/s, $N=600$ rpm; **c** $u_0=0.5$ m/s, $N=900$ rpm; **d** $u_0=1.5$ m/s, $N=600$ rpm. [94]



with the experimental data compared to the results of the 2D CFD model. However, to reduce the complexity of the 3D model, the packing was simplified without considering the effect of horizontal wire meshes which makes the results less realistic. Likewise, Zhang et al. [107] used the 3D CFD model to study the droplet breakup behavior using a single 3D layer of the packing. They did not study other attributes of liquid flow behavior in a fully developed region of RPB. Despite the complexities in the 3D model, Zhang et al. [88] tried to study the characteristics of liquid flow within the RPB using 3D

wire mesh packing (considering the effect of horizontal wire meshes) as shown in Fig. 9 and found that the computed flow pattern obtained as a result of 3D simulation showed a good agreement with the experimental data. However, the difference between the previous CFD data is within 30%, which they claimed is due to the difference in the packing structure.

Fig. 7 **a** Unstructured wire mesh [97], **b** structured wire mesh [98], **c** zigzag wire mesh [96], **d** foam packing [98] and **e** knitted wire mesh [98]



3.3 Effect of Different RPB Designs on the Hydrodynamics Parameters

The selection of the appropriate RPB design plays a vital role in the process design and optimization as the employment of the suitable configuration can save energy consumption

Table 6 Advantages and disadvantages of different RPB packing structures

Packing type	Advantages	Disadvantages	References
Structured/unstructured wire mesh	High mass transfer Can handle high viscosity liquids Can deal with a high flow rate of gases	High-pressure drop	[99]
Foam packing	Less costly	Low specific area High-pressure drop	[100]
Knit wire mesh	High mass transfer High surface area	High-pressure drop	[101]
Zigzag wire mesh	Higher mass transfer Low-pressure drop	Low effective gas–liquid interfacial area	[98]

and can improve the quality of the process. The design of the RPB can significantly affect the hydrodynamic parameters such as the pressure drop, liquid holdup, mean residence time and the liquid dispersion. Bai et al. [108] proposed a novel spherical design of the RPB as shown in the Fig. 10 and studied the effect of operational conditions on the liquid holdup, liquid mean residence time and the pressure drop. Furthermore, they reported that unlike the conventional RPB design, the rotational speed does not have any significant effect on the liquid holdup of the spherical RPB. Similarly, the pressure drop in the spherical RPB was found to be lower than the conventional RPB up to 35%. Therefore, the application of RPB at low rotational speed can reduce the energy consumption for any application. The application of spherical RPB is more suitable which requires very short liquid residence time. However, for the case when the rate of CO₂ absorption is low due to slow chemical reaction between the solvent and the CO₂ or the diffusion mechanism, this design of the RPB will not be a good selection due to its shorter residence time as compared to the conventional RPB.

The mass transfer efficiency of the RPB can also be intensified by adding any obstacle in the fluid path within the cavity zone of the RPB. Shi et al. [89] used the static baffles in the RPB to reduce the droplet size in the RPB for better dispersion and the mass transfer rate as shown in Fig. 11. The employment of the baffles in the RPB packing can reduce the flow path in the RPB and therefore also

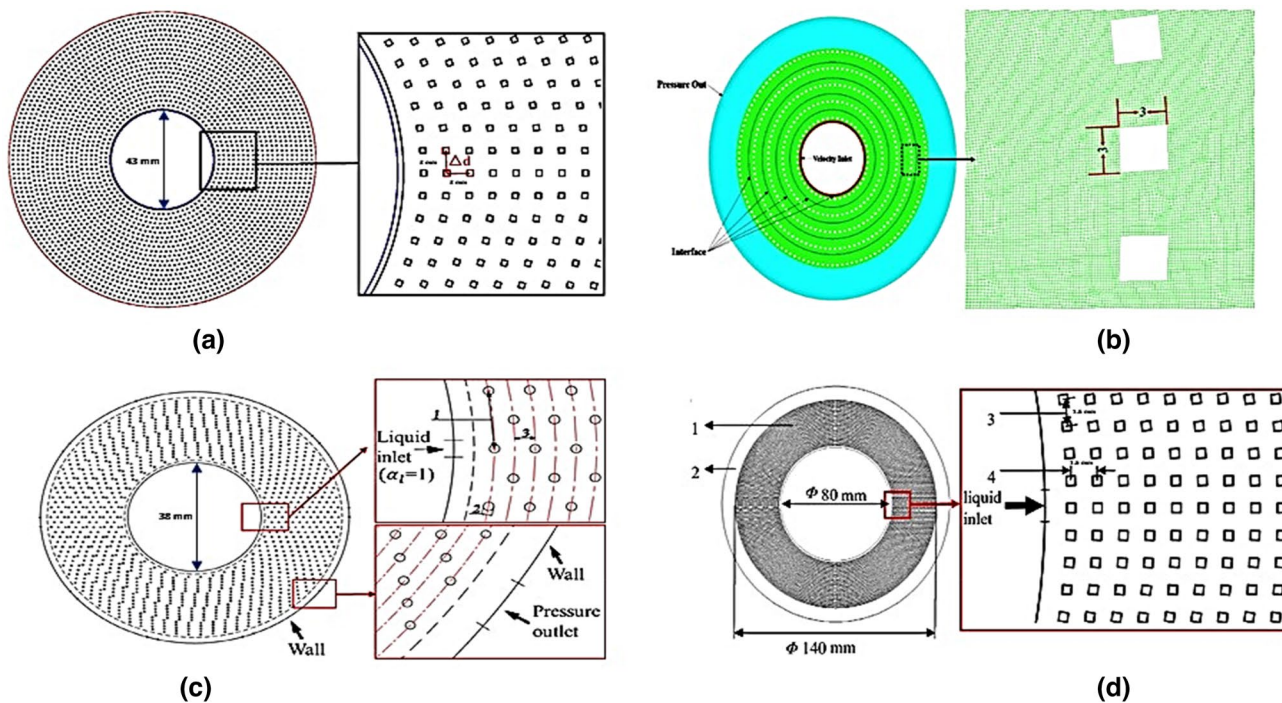


Fig. 8 2D CFD models with different packing structures and arrangement (a) square wire mesh packing with no stationary or cavity zone [91], b square wire mesh packing (3 mm × 3 mm) with cavity [104], c

circular wire mesh packing ($\varnothing=0.5$ mm) with no cavity zone [27] and d square wire mesh packing (0.5 mm × 0.5 mm) with cavity [102]

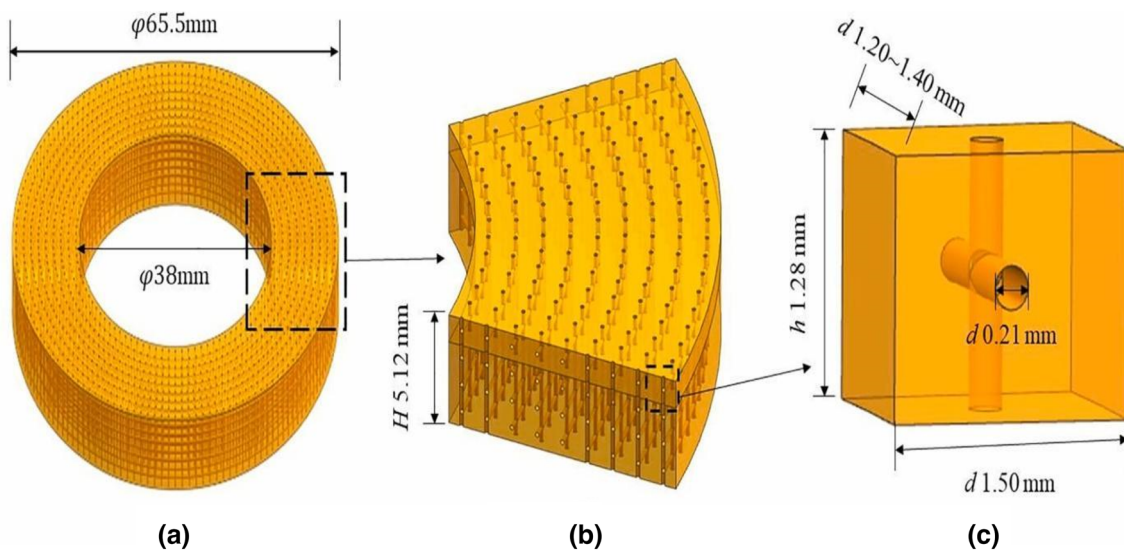


Fig. 9 3D model of RPB as proposed by Zhang et al. [88]: a entire flow domain, b cross-sectional view of the flow domain at 45° and c cross-sectional view of packing wire

reduce the mean residence time of the liquid [109, 110]. Another drawback that limits the application of RPB for the gas–liquid separation is the low angular slip velocity of the gas phase around the rotor. The use of static baffles in the RPB can cope with this drawback of RPB. Sung and Chen

[55] developed static baffles in RPB packing and found that using baffles in the packing can provide 117% more volumetric gas-transfer mass transfer coefficient as compared to the conventional RPB.

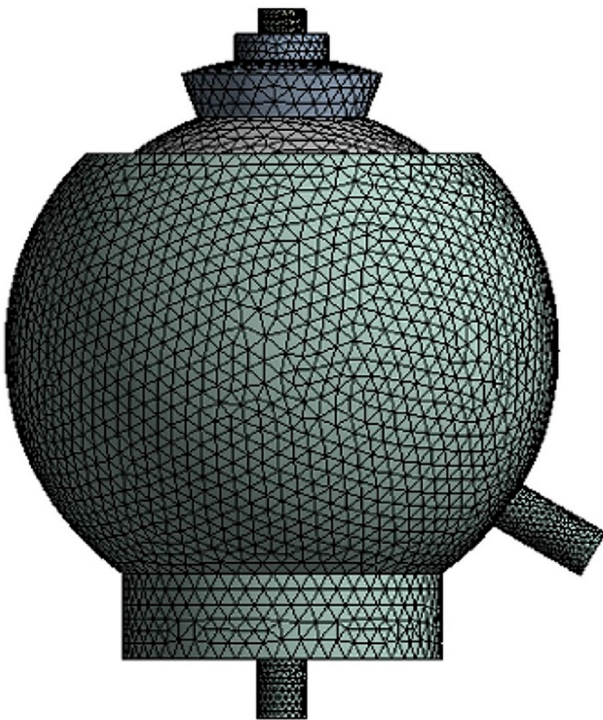


Fig. 10 Spherical RPB design proposed by Bai et al. [108]

3.4 Multiphase Phase Modeling in RPB

Multiphase models have been used extensively to simultaneously predict the interaction of more than one phase in the RPB. The Volume of Fluid (VOF) and the Eulerian model are the two most commonly used models to predict the flow characteristics (flow pattern) in the RPB.

3.4.1 Eulerian Approach

The Eulerian model has been used extensively for the CFD simulation of the various conventional reactors, such as packed bed reactor and fluidized bed reactor to predict the flow behavior and interaction of multiphase simultaneously. Some prominent advantages of this approach are (i) it does not require too small grids and therefore, can simulate the whole reactor by focusing on the fluid flow throughout the whole bed, (ii) more efficient for steady-state simulation and does not require high computational time and power, (iii) this model assumes both liquid and gaseous phases as individual phases [111]. However, the Eulerian model does not consider the drag forces between the gas–liquid, gas–solid and solid–liquid interfaces and thus is not able to predict the flow behavior around the packing of the RPB accurately [112, 113]. The porous media model has been used extensively in combination with the Eulerian model to predict the flow behavior in packed bed reactor [114, 115]. But due to the high porosity of wire mesh and cylindrical diameter of packing the porous media model cannot be used to predict the flow behavior and gas–liquid interaction in the RPB. Kołodziej and Łojewska [113] experimentally investigated the flow pattern through wire mesh packing and the conventional spherical packing and found that the flow through the wire meshing packing was entirely different from the spherical packing. There are very few studies reported so far, which have used the Eulerian Model for the CFD study of RPB. Lu et al. [112] developed a new porous media model for the CFD analysis of gas–liquid (air–water) two-phase system and found that this model cannot accurately predict the flow behavior within the RPB due to the assumption made to simplify the mathematical model. The application of the Eulerian model and the main findings are summarized

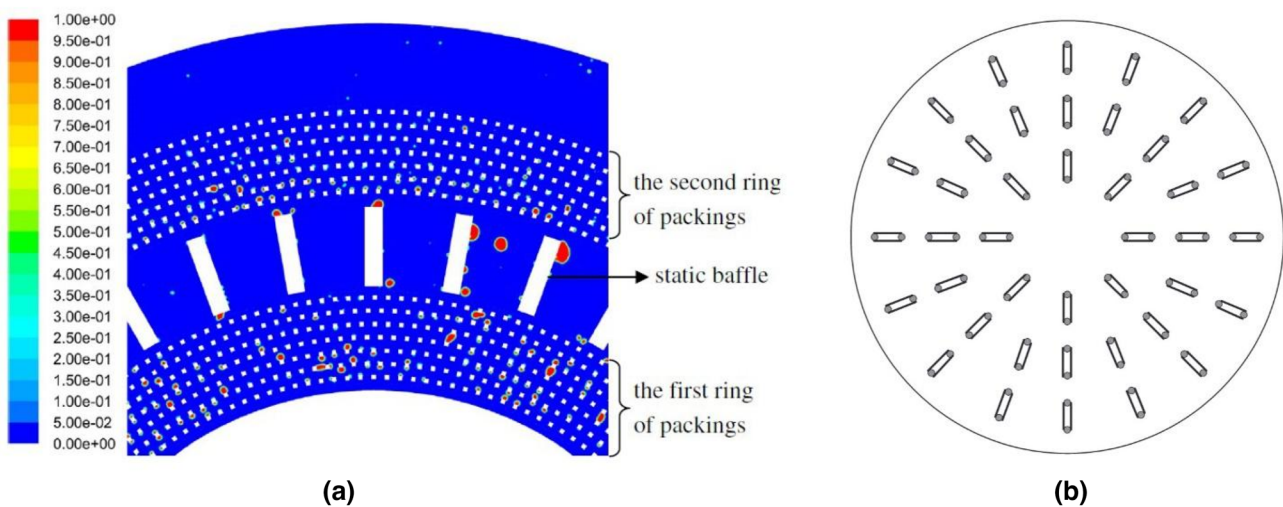


Fig. 11 a Contour of volume fraction with static baffles [89] and b blade baffle design [55]

in Table 7. Therefore, a more realistic model is required to be developed with minimum assumptions that can accurately predict the flow characteristics such as flow behavior and pattern and should include drag forces, interfacial area and can quantify the mass transfer in the RPB.

3.4.2 Volume of Fluid (VOF)

The volume of fluid (VOF) is one of the most capable multiphase models to analyze and track the gas–liquid interface in two-phase flow [102, 117]. This model uses a single set of momentum equations by considering both the liquid and the gas as a single phase and can predict the volume fraction of each fluid (gas and liquid) throughout the domain. The most highlighted advantages of this model are (i) the flow distribution of liquid can be analyzed using this model, (ii) the solution by this model is independent of interaction between different phases and (iii) can analyze all three types of flows, i.e., film flow, rivulet flow and droplet flow within the flow domain [93]. However, there are also some disadvantages associated with the application of this model, such as (i) it cannot be useful for the simulation of a whole reactor as it requires very tiny grids that need more time and computer resources to be simulated, (ii) VOF only emphasizes the numerical solution of liquid that flows along the packing side and (iii) it requires more computational time as compared to the Eulerian model [116]. Shi et al. [89] predicted the flow pattern of the RPB using the Volume of Fluid (VOF) model in combination with the sliding mesh model (SMM) and Reynolds stress model (RSM) to predict the liquid distribution (Fig. 12). They predicted the velocity fields and liquid volume distribution of fluid around the packing area within the RPB. The results showed that VOF was an effective model to understand the liquid–gas interface, which helped to predict the liquid–gas velocity distribution in the RPB.

Xie et al. [27] used Volume of Fluid (VOF) along with the SST k-omega model to investigate the liquid flow behavior in RPB for CO₂ (physical) absorption. The results exhibited that the VOF model could successfully simulate the liquid flow pattern by tracking the gas–liquid interface around the packed area of RPB. Based on the

validation of simulated data, Xie et al. [27] concluded that the VOF model has promising potential and is capable to analyze the hydrodynamics of industrial RPB using 3D CFD modeling. Ouyang et al. [106] and Guo et al. [103] used realized k-epsilon model in combination with the VOF model to simulate the gas–liquid phases in RPB. They found it an effective approach to capture the gas–liquid interfaces and analyze instantaneous flow information such as liquid film and droplet flow in the RPB. Yang et al. [93] employed the VOF model to study the gas–liquid mass transfer in the RPB. They concluded that the gas–liquid interface cannot be predicted accurately because the computational grids in their conducted study were not small enough to capture the gas–liquid interfaces accurately. The reported research shows that Volume of Fluid (VOF) is the most suitable model to investigate the hydrodynamics of multiphase flow in the RPB [89, 93, 102, 118].

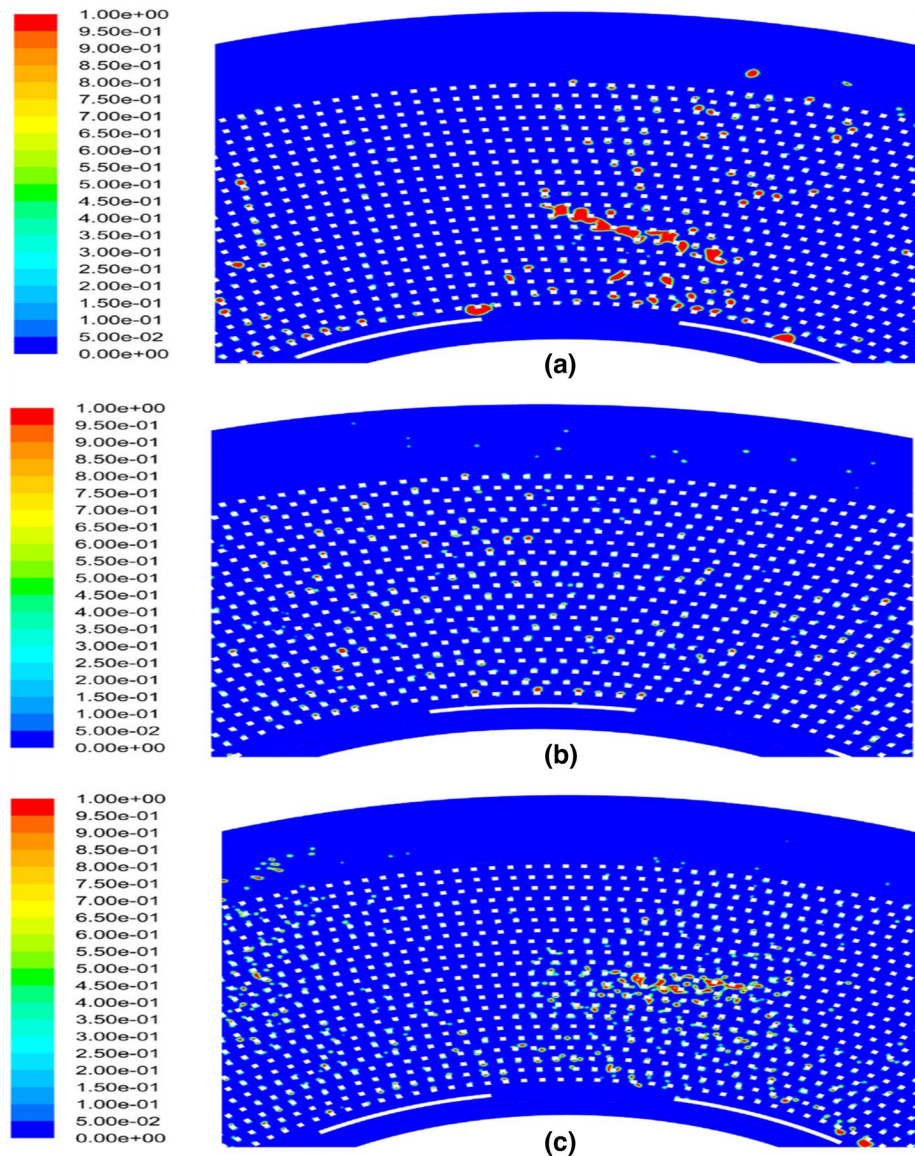
3.4.3 Turbulence Modeling in RPB

There are several factors that affect the accuracy of the CFD results. The selection of an appropriate turbulence model is one among them, and the model selection should be based on its adaptability [38]. The standard k- ϵ , SST k- ω , Reynolds stress model (RSM), and the Detached Eddy Simulation Turbulence Model (DES) are the most commonly employed models for turbulent flow prediction. Each turbulence model has its own limitation and uses the different set of boundary conditions. Guo et al. [102] studied the micro-mixing efficiency in RPB using Reynolds Stress Model (RSM) by simulating the volume fraction of liquid and the concentration distribution. The effect of rotational speed and liquid velocity were studied to investigate their influence on the micro-mixing efficiency of the RPB. The simulated results exhibited good agreement with the experimental data. As the Reynolds Stress Model (RSM) uses five (2D flow) and seven (3D flow) additional equations, it demands more time and computational memory [119]. Xie et al. [27] applied the Standard and SST k-omega model for the closure of the Navier–Stokes equation for simulating the physical absorption of CO₂ in RPB using MEA as a solvent. The liquid holdup predicted by the Standard and SST k-omega models

Table 7 Main findings of the Eulerian model

Sr. no.	Phases	Main findings	References
1	Gas–liquid	Eulerian model, in combination with the developed porous media model does not predict the flow pattern around the packing	[112]
2	Gas–liquid	The porous media model is based on liquid film flow assumption and insufficient information in the mathematical model limits the credibility of predicted flow characteristics	[116]
3	Gas–liquid	The Eulerian–Lagrangian approach only predicts the droplet characteristics of H ₂ S in RPB and does not explain well the Ligament flow	[94]

Fig. 12 The maldistribution of the liquid phase in the packing area ($t=0.5$ s): **a** $N=500$ rpm, $u=0.5$ m/s; **b** $N=900$ rpm, $u=0.5$ m/s; and **c** $N=900$ rpm, $u=2$ m/s. [89]



was within 5% of the holdup obtained by the RSM model. Yang et al. [120] employed the Realizable k -epsilon and Standard k -epsilon turbulence models to optimize the single (gas) phase flow in the RPB. The standard k -epsilon model showed a better agreement with the experimental data as compared to the Realizable k -epsilon model. However, the agreement was good only for low rotational speed, i.e., rotational speed < 1000 rpm. Table 8 summarizes the multiphase and turbulence model used so far for the CFD analysis of RPB.

3.4.4 Rotating Reference Frame

The rotational speed of the RPB has a significant effect on the hydrodynamics of the RPB. Therefore, it is necessary to adopt a suitable rotating reference frame model that can

incorporate the effect of rotation and can be proven an efficient model in investigating the hydrodynamics of RPB. The sliding mesh model (SMM) is a completely unsteady method that can be employed effectively for the CFD analysis of RPB. Shi et al. [89] used SMM to visualize the liquid pattern in the RPB by generating a dense gravity environment using this model and found that the simulated results showed a good agreement with the experimental data. On the other hand, researchers have also used the moving reference frame for considering the rotation of the RPB [27, 105, 106, 121]. Both the single rotating reference frame and multiple reference frame have been used for this purpose. For the CFD geometry having more than two interfaces, multiple reference frame is the only available model to employ for the unsteady state simulation. For example, Lui et al. [98] concluded that moving reference frame is an effective

Table 8 Multiphase and Turbulence Model used for CFD study of RPB

Packing specification	Multiphase model	Turbulence model	Phases	Geometry type	Boundary conditions	Grid size	Flow time (s)	Main findings	References
Packing type: wire mesh	VOF	Reynold stress model	liquid	2D	Liquid velocity: 0.25–1.25 m/s Rotational speed: 500–900 RPMs	1.42 M	0.5	The VOF model is an effective modeling for capturing the interface between the gas and liquid phase.	[89]
Packing type: wire mesh	VOF	Reynold stress model	Gas–liquid	2D	Liquid Velocity: 0.3–0.7 m/s Rotational speed: 500–900 RPMs	1.42 M	0.5	The CFD results show a good agreement with the experimental data. The CFD model can be adopted to calculate the micromixing efficiency of the RPB.	[102]
Packing type: wire mesh	VOF	Realizable k-epsilon	Gas–liquid	3D	Liquid velocity: 0.25–0.75 m/s Rotational speed: 400–1200 RPMs	1.62 M	0.5	The CFD results using 3D geometry better predict the hydrodynamics of the RPB as compared to the 2D geometry. The mean residence time of 3D geometry was 10% higher than that of 2D geometry.	[103]
Packing type: wire mesh Void fraction: 0.94	VOF	Reynold stress model	Gas–liquid	2D	Liquid flow rate: 75–150 L/h Rotational speed: 600–1200 RPMs	0.16 M	5	The removal efficiency by CFD simulations was compared with the experimental data and there was a deviation of only $\pm 5\%$ CFD can effectively predict the fluid dynamics and the mass transfer performance of the RPB.	[93]

Table 8 (continued)

Packing specification	Multiphase model	Turbulence model	Phases	Geometry type	Boundary conditions	Grid size	Flow time (s)	Main findings	References
Packing type: wire mesh	VOF	Reynold stress model	Gas-Liquid	2D	Liquid velocity: 0.5–2.0 m/s Rotational speed: 200–1000 RPMs	2.3 M	0.05–0.005	The correlation between the droplet size, rotational speed and the liquid velocity developed using CFD simulation showed a good agreement with the experimental data. The maximum deviation between the CFD results and the experimental data was found to be $\pm 15\%$	[104]
Packing type: wire mesh	VOF	Realizable k-epsilon	Gas	2D, 3D	Gas flow rate: 10–50 m ³ /h Rotational speed: 600–1400 RPMs	2D: 0.1 M 3D: 0.62 M	–	The hydrodynamics of multi-liquid inlet RPB can be understood using 3D CFD simulations. The CDF model was validated using the CFD simulation values of pressure drop and the experimental data. The CFD simulations can be used for the structural optimization of the RPB.	[105]

Table 8 (continued)

Packing specification	Multiphase model	Turbulence model	Phases	Geometry type	Boundary conditions	Grid size	Flow time (s)	Main findings	References
Packing type: wire mesh	VOF	Realizable k-epsilon	Gas-liquid	2D	Liquid flow rate: 80–1000 L/h Rotational speed: 1000–2500 RPMs	0.2 M	0.5–0.05	The CFD simulation was successfully employed to determine the mean residence time (MRT) by residence time distribution data. Time step size $<1 \times 10^{-6}$ was not able to predict the hydrodynamics at higher rotation speed, i.e., $N > 2000$ RPMs. CFD model showed a good validation with the experimental data.	[106]
Packing type: stainless steel wire mesh packing Specific surface area: 385 1/m Void fraction: 0.94	VOF	Realizable k-epsilon	Gas	3D	Gas flow rate: m ³ /h Rotational speed: 400–1200 RPMs	9.3 M	–		[98]
Packing type: wire mesh packing Void fraction: 0.84 Specific surface area: 546.5 1/m	VOF	SST k-omega	Gas-Liquid	3D	Gas flow rate: 0.005–0.016 m/s Contact angle: 30–120° Rotational speed: 1000–2500 RPMs	1.4–2.42 M	–	A dense mesh, i.e., 2.42 M, was required when the centrifugal acceleration of the RPB was more than 100 m/s ² . Increasing the rotational speed does not significantly increase the effective interfacial area. Increasing the liquid flow rate have negative impact on the specific surface area of the liquid.	[50]

Table 8 (continued)

Packing specification	Multiphase model	Turbulence model	Phases	Geometry type	Boundary conditions	Grid size	Flow time (s)	Main findings	References
Packing type: isotropic metal foam Specific surface area: 2800 1/m	–	SST k-epsilon RNG k-epsilon	Gas	3D	Gas flow rate: 20–60 m ³ /h Rotational speed: 150–1200 RPMs	1.65 M	–	RNG k-epsilon required long computational time as compared to the SST k-epsilon. However, the difference in the results was not significant. The simulation results started to deviate from the experimental data at higher gas flow rate. The turbulence models were unable to describe the flow behavior of the gas within the 3D CFD model.	[95]
Packing type: wire screen packing	Eulerian (porous media) model	–	Gas–liquid	2D	Rotational speed: 600–1200 RPMs	–	–	Eulerian model in combination with the newly developed porous media approach, is more effective than the previously reported conventional porous media models	[112]

Table 8 (continued)

Packing specification	Multiphase model	Turbulence model	Phases	Geometry type	Boundary conditions	Grid size	Flow time (s)	Main findings	References
Packing type: wire mesh packing Specific surface area: 663 1/m Void fraction: 0.8	Eulerian (porous media) model	–	Gas–Liquid	2D	Rotational speed: 600–1150 RPMs	–	–	The Eulerian model required less computational power as compared to the volume VOF model. The mass transfer modelling was employed for the CO ₂ absorption in the MEA using 2D CFD model. However, a better understanding can be developed regarding hydrodynamics and the mass transfer rate with the 3D CFD model.	[116]
Packing type: wire mesh packing	Eulerian–Lagrangian	Standard K-epsilon	Gas–liquid	3D	Rotational Speed: 300–900 RPMs	4.3 M	0.04	The mean residence time, average velocity and the droplet size of the solvent were calculated to predict the mass transfer efficiency of the RPB for the H ₂ S absorption using the CFD simulations. The results showed a good agreement with the experimental data. The minimum droplet size was obtained at the highest rotational speed under consideration. The CFD model using Eulerian–Lagrangian has the potential to predict the droplet characteristics of the solvent in the RPB.	[94]

Table 8 (continued)

Packing specification	Multiphase model	Turbulence model	Phases	Geometry type	Boundary conditions	Grid size	Flow time (s)	Main findings	References
Packing type: Stainless steel wire mesh Void fraction: 0.92	Eulerian model	Standard K-epsilon	Gas-Liquid	3D	Gas flow rate: 150–350 L/h Rotational speed: 600–2200 RPMs	–	20	Numerical modeling of pressure drop by CFD revealed that the pressure drop by the novel spherical rotor is 20–30% less than that of conventional RPB. For effective performance and the optimization of spherical rotor RPB, the space in the outer cavity zone may be considered for fluid buffering. During the RPB application, the high rotor speed should not be opted to avoid the equipment failure due to over pressure drop.	[108]

way to study the flow behavior at the rotor-cavity interface. However, when there is only a single interface, single rotating reference frame can be adapted to study the liquid flow characteristics. Xie et al. [27] employed a single reference frame along with a UDF to control the movement of the inlet to investigate the hydrodynamics of the RPB and concluded that the moving reference frame (MRF) is a useful method when studying the flow behavior at rotor-cavity interface. Both MRF and SMM are found to be effective when simulating the rotating packed bed. However, if the geometry contains more than one zone i.e., stationary and rotating zones, the MRF is the only model available that can be employed to predict the hydrodynamics of gas-liquid in RPB.

3.4.5 Reactive CFD Modeling of CO₂ Absorption

There exists very limited data for the CFD analysis of the reactive absorption of CO₂ which incorporates the effect of chemical reaction on the mass transfer rate of the RPB. Sebastia-Saez et al. [122] studied the mass transfer rate by employing micro-scale CFD modeling of CO₂ absorption in packed bed column using the volume of fluid multiphase model. The formation of the carbamate (RNH⁺COO⁻) was considered as the rate-controlling step, which described the complete reaction kinetics of the chemical absorption of CO₂. The consumption of the MEA and production of carbamate during the chemical reaction between MEA and CO₂ was incorporated into the source terms using the UDF. Considering the formation of the carbamate (RNH⁺COO⁻) as an irreversible reaction, the rate of the reaction was calculated by the following equation:

$$R_{\text{reaction}} = K[\text{CO}_2][\text{RNH}_2] \quad (10)$$

where, K was the forward rate of reaction, which is 24,984 m³kmol⁻¹s⁻¹ [122, 123]. Gbadago et al. [124] studied the reactive absorption of CO₂ in industrial packed bed adsorber using the Eulerian (porous media approach) multiphase model in combination with standard k-epsilon turbulence model. The simulated results of pressure-drop and absorption efficiency were compared with the experimental data of the pilot plant absorber. The simulated results showed 5.2% deviation from the experimental data. However, no attempt has been made to study the effect of reaction on the absorption of CO₂ in the RPB.

To sum up the discussion, CFD has found its successful application to study the flow characteristics of gas and liquid in the RPB. Unlike the experimental approach, this approach does not require sophisticated engineering tools to predict the hydrodynamics. In addition, a single unit of RPB for the experimental study does not allow any modification in the physical structure

of the RPB such as change in packing type, number of injecting nozzles, size of injecting nozzles and the RPB configuration, etc. to study the effect of these parameters on the hydrodynamics of the RPB. Similarly, to scale up the laboratory setup to study the flow characteristics and mass transfer performance of RPB for the industrial application is a time taking approach. On the other hand, CFD is capable of handling these sorts of challenges. Moreover, CFD provides both the visual contours and quantified parameters for the hydrodynamics parameters which provide a better insight of the flow behavior which is favorable attribute for the designing and optimization of the RPB. The comparison of CFD results and the experimental data revealed that CFD has the ability to efficiently predict the mass transfer performance and the hydrodynamics of the RPB on lab scale as well as on the industrial scale. However, predictive potential of CFD is very sensitive to the selection of turbulence model, number of grids and the geometric configurations, i.e., 2D or 3D.

4 Conclusion and Future perspective

The conclusion of the review is as follows.

- The experimental methods have been employed widely to study the hydrodynamics of RPB. However, this approach is expensive and has a lot of engineering problems, such as the installation of technical instruments in RPB for capturing the hydrodynamics of RPB. On the other hand, the analytical correlations used with the experimental methods are based on assumptions that effect the prediction of the hydrodynamics of RPB.
- The application of the rotating packed bed reactor is a promising approach to control the depletion of CO₂ into the atmosphere. The process of CO₂ absorption can be more cost-effective and efficient by the optimization of process parameters such as rotating speed, solvent concentration, contact angle and the solvent inlet velocity. Mass transfer is one of the most important aspects while considering and optimizing the efficiency of RPB which can be quantified by incorporating an appropriate mass transfer model into the governing equations.
- Among various approaches to study the hydrodynamics of the RPB, CFD is the most effective way to study and investigate the hydrodynamic parameters such as liquid hold up, liquid residence time, pressure drop, etc. The 3D packing structure of RPB is complex, therefore, assumptions have been made in the past to simplify the CFD model. In order to understand the actual hydrodynamics of RPB, 3D CFD model with

minimum possible assumptions is required to develop for the in-depth CFD analysis of RPB.

- d. The Volume of Fluid (VOF) is the most effective model to predict the volume fraction of each CO₂ and solvent throughout the flow domain. However, the VOF model requires more computational time as compared to the Eulerian model. Eulerian model in combination with the suitable porous media model can be used to reduce the computational time. However, there exists no suitable porous media that can be used to model the porous mesh packing structure of RPB.
- e. The selection of a suitable turbulence model is necessary to accurately predict the flow for its adaptability. Reynold Stress Model (RSM) is the most accurate turbulence model for the CFD analysis of RPB. Moreover, this model requires much more computational time as compared to its counterparts. On the other hand, there exist two-equation models such as k-omega and k-epsilon which have also shown a good agreement with the experimental data.
- f. The validation of the CFD model for the analysis of CO₂ absorption is a great challenge nowadays. As there exist no data in the literature which contains the experimental data of CO₂ absorption that can be utilized for the model validation.
- g. The absorption of CO₂ is a physio-chemical process. All the previously reported studies have only considered the physical absorption of the CO₂ to study the flow characteristics of CO₂ and solvent. However, to accurately predict the flow behavior of fluid in RPB, reactive absorption of CO₂ must need to be considered and the effect of reaction on mass transfer within the reactor must need to be studied in detail.
- h. The mass transfer rate in the RPB depends on different RPB configurations. The detail understanding of the fluid behavior in different configurations need to be developed yet to practically utilize the potential of the RPB for the selected applications.

Acknowledgements This project was sponsored by the Ministry of Higher Education, Malaysia under Fundamental Research Grant Scheme (FRGS), Contract number: FRGS/1/2018/TK02/CURTIN/02/4

Funding Open Access funding enabled and organized by CAUL and its Member Institutions.

Open Access This article is licensed under a Creative Commons Attribution 4.0 International License, which permits use, sharing, adaptation, distribution and reproduction in any medium or format, as long as you give appropriate credit to the original author(s) and the source, provide a link to the Creative Commons licence, and indicate if changes were made. The images or other third party material in this article are included in the article's Creative Commons licence, unless indicated otherwise in a credit line to the material. If material is not included in the article's Creative Commons licence and your intended use is not permitted by statutory regulation or exceeds the permitted use, you will

need to obtain permission directly from the copyright holder. To view a copy of this licence, visit <http://creativecommons.org/licenses/by/4.0/>.

References

1. End Coal | Climate Change (2020) <https://endcoal.org/climate-change/>. Accessed 09 Oct 2020
2. Feron PHM (2016) Introduction. In: Feron PHM (ed) Absorption-based post-combustion capture of carbon dioxide. Woodhead Publishing, Cambridge, pp 3–12
3. Mukherjee A, Okolie JA, Abdelrasoul A, Niu C, Dalai AK (2019) Review of post-combustion carbon dioxide capture technologies using activated carbon. *J Environ Sci* 83:46–63. <https://doi.org/10.1016/j.jes.2019.03.014>
4. Jiang G et al (2015) A new mesoporous amine-TiO₂ based pre-combustion CO₂ capture technology. *Appl Energy* 147:214–223. <https://doi.org/10.1016/j.apenergy.2015.01.081>
5. Scholes CA, Ho MT, Wiley DE, Stevens GW, Kentish SE (2013) Cost competitive membrane-cryogenic post-combustion carbon capture. *Int J Greenh Gas Control* 17:341–348. <https://doi.org/10.1016/j.ijggc.2013.05.017>
6. Zhong DL, Sun DJ, Lu YY, Yan J, Le Wang J (2014) Adsorption-hydrate hybrid process for methane separation from a CH₄/N₂/O₂ gas mixture using pulverized coal particles. *Ind Eng Chem Res* 53(40):15738–15746. <https://doi.org/10.1021/ie502684j>
7. Moioli S, Giuffrida A, Gamba S, Romano MC, Pellegrini L, Lozza G (2014) Pre-combustion CO₂ capture by MDEA process in IGCC based on air-blown gasification. *Energy Procedia* 63:2045–2053. <https://doi.org/10.1016/j.egypro.2014.11.220>
8. Creamer AE, Gao B (2015) Adsorbents for CO₂ capture. Springer, Cham, pp 25–41
9. Ding S, Liu Y (2020) Adsorption of CO₂ from flue gas by novel seaweed-based KOH-activated porous biochars. *Fuel* 260:116382. <https://doi.org/10.1016/j.fuel.2019.116382>
10. Song C, Liu Q, Deng S, Li H, Kitamura Y (2019) Cryogenic-based CO₂ capture technologies: State-of-the-art developments and current challenges. *Renew Sustain Energy Rev* 101:265–278. <https://doi.org/10.1016/j.rser.2018.11.018>
11. Norahim N, Yaisanga P, Faungnawakij K, Charinpanitkul T, Klaysom C (2018) Recent membrane developments for CO₂ separation and capture. *Chem Eng Technol* 41(2):211–223. <https://doi.org/10.1002/ceat.201700406>
12. Sreedhar I, Nahar T, Venugopal A, Srinivas B (2017) Carbon capture by absorption—path covered and ahead. *Renew Sustain Energy Rev* 76:1080–1107. <https://doi.org/10.1016/j.rser.2017.03.109>
13. Ban ZH, Keong LK, Shariff AM (2014) Physical absorption of CO₂ capture: a review. *Adv Mater Res* 917:134–143. <https://doi.org/10.4028/www.scientific.net/AMR.917.134>
14. Wang M, Lawal A, Stephenson P, Sidders J, Ramshaw C, Yeung H (2011) Post-combustion CO₂ capture with chemical absorption: a state-of-the-art review. *Chem Eng Res Des* 89:1609–1624
15. Borhani TN, Oko E, Wang M (2019) Process modelling, validation and analysis of rotating packed bed stripper in the context of intensified CO₂ capture with MEA. *J Ind Eng Chem* 75:285–295. <https://doi.org/10.1016/j.jiec.2019.03.040>
16. Li T, Keener TC (2016) A review: desorption of CO₂ from rich solutions in chemical absorption processes. *Int J Greenh Gas Control* 51:290–304. <https://doi.org/10.1016/j.ijggc.2016.05.030>
17. Mota-Martinez MT, Hallett JP, MacDowell N (2017) Solvent selection and design for CO₂ capture-how we might have been missing the point. *Sustain Energy Fuels* 1(10):2078–2090. <https://doi.org/10.1039/c7se00404d>

18. Dhoke C, Zaabou A, Cloete S, Amini S (2021) Review on reactor configurations for adsorption-based CO₂ capture. *Ind Eng Chem Res* 60(10):3779–3798. https://doi.org/10.1021/ACS.IECR.0C04547/SUPPL_FILE/IE0C04547_SI_001.PDF
19. Abanades JC et al (2015) Emerging CO₂ capture systems. *Int J Greenh Gas Control* 40:126–166. <https://doi.org/10.1016/J.IJGGC.2015.04.018>
20. Li L, Xie W, Zhang Z, Zhang S (2020) Pressure drop in packed beds with horizontally or vertically stratified structure. *Nucl Eng Technol* 52(11):2491–2498. <https://doi.org/10.1016/J.NET.2020.05.001>
21. Ajua Mustafa NF, Shariff AM, Tay WH, Halim HNA, Yusof SMM (2020) Mass transfer performance study for CO₂ absorption into non-precipitated potassium carbonate promoted with glycine using packed absorption column. *Sustainability* 12(9):3873. <https://doi.org/10.3390/SU12093873>
22. Chikukwa A, Enaasen N, Kvamsdal HM, Hillestad M (2012) Dynamic modeling of post-combustion CO₂ capture using amines—a review. *Energy Procedia* 23:82–91. <https://doi.org/10.1016/J.EGYPRO.2012.06.063>
23. Riboldi L, Bolland O (2015) Evaluating pressure swing adsorption as a CO₂ separation technique in coal-fired power plants. *Int J Greenh Gas Control* 39:1–16. <https://doi.org/10.1016/J.IJGGC.2015.02.001>
24. Xie P, Lu X, Ingham D, Ma L, Pourkashanian M (2017) Mass transfer characteristics of the liquid film flow in a rotating packed bed for CO₂ capture: a micro-scale CFD analysis. *Energy Procedia* 142:3407–3414. <https://doi.org/10.1016/j.egypro.2017.12.478>
25. Yan ZY, Lin C, Ruan Q (2014) Dynamics of droplets and mass transfer in a rotating packed bed. *AIChE J* 60(7):2705–23
26. Liu YZ, Li ZH, Chu GW, Shao L, Luo Y, Chen JF (2020) Liquid-solid mass transfer in a rotating packed bed reactor with structured foam packing. *Chin J Chem Eng* 28(10):2507–12
27. Xie P, Lu X, Yang X, Ingham D, Ma L, Pourkashanian M (2017) Characteristics of liquid flow in a rotating packed bed for CO₂ capture: a CFD analysis. *Chem Eng Sci* 172:216–229. <https://doi.org/10.1016/j.ces.2017.06.040>
28. Visscher F, van der Schaaf J, Nijhuis TA, Schouten JC (2013) Rotating reactors—a review. *Chem Eng Res Des* 91(10):1923–1940. <https://doi.org/10.1016/J.CHERD.2013.07.021>
29. Lin CC, Chen BC, Chen YS, Hsu SK (2008) Feasibility of a cross-flow rotating packed bed in removing carbon dioxide from gaseous streams. *Sep Purif Technol* 62(3):507–512. <https://doi.org/10.1016/J.SEPUR.2008.02.019>
30. Wang Z, Yang T, Liu Z, Wang S, Gao Y, Wu M (2019) Mass transfer in a rotating packed bed: a critical review. *Chem Eng Process Process Intensif* 139:78–94. <https://doi.org/10.1016/J.CEP.2019.03.020>
31. Chen YS (2011) Correlations of mass transfer coefficients in a rotating packed bed. *Ind Eng Chem Res* 50(3):1778–1785. <https://doi.org/10.1021/ie101251z>
32. Yang Y et al (2015) A noninvasive X-ray technique for determination of liquid holdup in a rotating packed bed. *Chem Eng Sci* 138:244–255. <https://doi.org/10.1016/J.CES.2015.07.044>
33. Liu Y et al (2019) CFD simulation and high-speed photography of liquid flow in the outer cavity zone of a rotating packed bed reactor. *Ind Eng Chem Res* 58(13):5280–5290. <https://doi.org/10.1021/acs.iecr.8b05718>
34. Yan ZY, Lin C, Ruan Q (2012) Hydrodynamics in a rotating packed bed. I. A novel experimental method. *Ind Eng Chem Res* 51(31):10472–10481. <https://doi.org/10.1021/IE202257T>
35. Bongo D, Mouangué Nanimina A, Kadjangaba E, Champagne J-Y (2019) Experimental study of hydrodynamics in the aquarium using PIV method. *Am J Energy Eng* 7(4):74. <https://doi.org/10.11648/j.ajee.20190704.11>
36. Burns JR, Ramshaw C (1996) Process intensification: visual study of liquid maldistribution in rotating packed beds. *Chem Eng Sci* 51(8):1347–1352. [https://doi.org/10.1016/0009-2509\(95\)00367-3](https://doi.org/10.1016/0009-2509(95)00367-3)
37. Wen Z-N et al (2023) Liquid flow behavior in the concentric mesh packing with novel fiber cross-sectional shape in a rotating packed bed. *Chem Eng J* 451:139094. <https://doi.org/10.1016/J.CEJ.2022.139094>
38. Guo F, Zheng C, Guo K, Feng Y, Gardner NC (1997) Hydrodynamics and mass transfer in cross-flow rotating packed bed. *Chem Eng Sci* 52(21–22):3853–3859. [https://doi.org/10.1016/S0009-2509\(97\)00229-7](https://doi.org/10.1016/S0009-2509(97)00229-7)
39. Wenzel D, Górák A (2018) Review and analysis of micromixing in rotating packed beds. *Chem Eng J* 345:492–506. <https://doi.org/10.1016/J.CEJ.2018.03.109>
40. Groß K et al (2019) Analysis of flow patterns in high-gravity equipment using gamma-ray computed tomography. *Chem-Ing-Tech* 91(7):1032–1040. <https://doi.org/10.1002/CITE.201800085>
41. Burns JR, Jamil JN, Ramshaw C (2000) Process intensification: operating characteristics of rotating packed beds—determination of liquid hold-up for a high-voidage structured packing. *Chem Eng Sci* 55(13):2401–2415. [https://doi.org/10.1016/S0009-2509\(99\)00520-5](https://doi.org/10.1016/S0009-2509(99)00520-5)
42. Lin CC, Chen YS, Liu HS (2000) Prediction of liquid holdup in countercurrent-flow rotating packed bed. *Chem Eng Res Design* 78(3):397–403
43. Hendry JR, Lee JGM, Attidekou PS (2020) Pressure drop and flooding in rotating packed beds. *Chem Eng Process Process Intensif* 151:107908. <https://doi.org/10.1016/J.CEP.2020.107908>
44. Burns JR, Jamil JN, Ramshaw C (2000) Process intensification: Operating characteristics of rotating packed beds—determination of liquid hold-up for a high-voidage structured packing. *Chem Eng Sci* 55(13):2401–2415. [https://doi.org/10.1016/S0009-2509\(99\)00520-5](https://doi.org/10.1016/S0009-2509(99)00520-5)
45. Chen YH et al (2003) Modeling ozone contacting process in a rotating packed bed. *Ind Eng Chem Res* 43(1):228–236. <https://doi.org/10.1021/IE030545C>
46. Guo K, Guo F, Feng Y, Chen J, Zheng C, Gardner NC (2000) Synchronous visual and RTD study on liquid flow in rotating packed-bed reactor. *Chem Eng Sci* 55(9):1699–1706. [https://doi.org/10.1016/S0009-2509\(99\)00369-3](https://doi.org/10.1016/S0009-2509(99)00369-3)
47. Li WL et al (2019) CFD analysis of gas flow characteristics and residence time distribution in a rotating spherical packing bed. *Ind Eng Chem Res* 58(47):21717–21729. <https://doi.org/10.1021/ACS.IECR.9B03625>
48. Emami-Meibodi M, Soleimani M, Bani-Najarian S (2018) Toward enhancement of rotating packed bed (RPB) reactor for CaCO₃ nanoparticle synthesis. *Int Nano Lett* 8:189–199. <https://doi.org/10.1007/s40089-018-0244-4>
49. Keyvani M (1989) Operating characteristics of rotating beds
50. Xie P et al (2019) A mesoscale 3D CFD analysis of the liquid flow in a rotating packed bed. *Chem Eng Sci* 199:528–545. <https://doi.org/10.1016/J.CES.2019.01.038>
51. Zhang W, Xie P, Li Y, Teng L, Zhu J (2020) Hydrodynamic characteristics and mass transfer performance of rotating packed bed for CO₂ removal by chemical absorption: a review. *J Nat Gas Sci Eng* 79:103373. <https://doi.org/10.1016/j.jngse.2020.103373>
52. Said W, Nemer M, Clodic D (2011) Modeling of dry pressure drop for fully developed gas flow in structured packing using CFD simulations. *Chem Eng Sci* 66(10):2107–2117. <https://doi.org/10.1016/J.CES.2011.02.011>
53. Neumann K, Hunold S, Skiborowski M, Górák A (2017) Dry pressure drop in rotating packed beds—systematic experimental studies. *Ind Eng Chem Res* 56(43):12395–12405. https://doi.org/10.1021/ACS.IECR.7B03203/SUPPL_FILE/IE7B03203_SI_001.PDF

54. Lin CC, Jian GS (2007) Characteristics of a rotating packed bed equipped with blade packings. *Sep Purif Technol* 54(1):51–60. <https://doi.org/10.1016/j.seppur.2006.08.006>
55. Der Sung W, Chen YS (2012) Characteristics of a rotating packed bed equipped with blade packings and baffles. *Sep Purif Technol* 93:52–58. <https://doi.org/10.1016/J.SEPPUR.2012.03.033>
56. Li X, Liu Y (2010) Characteristics of fin baffle packing used in rotating packed bed. *Chin J Chem Eng* 18(1):55–60. [https://doi.org/10.1016/S1004-9541\(08\)60323-7](https://doi.org/10.1016/S1004-9541(08)60323-7)
57. Yang K, Chu G, Zou H, Sun B, Shao L, Chen JF (2011) Determination of the effective interfacial area in rotating packed bed. *Chem Eng J* 168(3):1377–1382. <https://doi.org/10.1016/J.CEJ.2011.01.100>
58. Im D, Jung H, Lee JH (2020) Modeling, simulation and optimization of the rotating packed bed (RPB) absorber and stripper for MEA-based carbon capture. *Comput Chem Eng* 143:107102. <https://doi.org/10.1016/J.COMPCHEMENG.2020.107102>
59. Billet R, Schultes M (1999) Prediction of mass transfer columns with dumped and arranged packings: updated summary of the calculation method of billet and schultes. *Chem Eng Res Des* 77(6):498–504. <https://doi.org/10.1205/026387699526520>
60. Tsai CY, Chen YS (2015) Effective interfacial area and liquid-side mass transfer coefficients in a rotating bed equipped with baffles. *Sep Purif Technol* 144:139–145. <https://doi.org/10.1016/J.SEPPUR.2015.02.008>
61. Luo Y, Chu GW, Zou HK, Zhao ZQ, Dudukovic MP, Chen JF (2012) Gas–liquid effective interfacial area in a rotating packed bed. *Ind Eng Chem Res* 51(50):16320–16325. <https://doi.org/10.1021/IE302531J>
62. Onda K, Takeuchi H, Okumoto Y (1968) Mass transfer coefficients between gas and liquid phases in packed columns. *J Chem Eng Japan* 1(1):56–62. <https://doi.org/10.1252/JCEJ.1.56>
63. Chu GW, Sang L, Du XK, Luo Y, Zou HK, Chen JF (2015) Studies of CO₂ absorption and effective interfacial area in a two-stage rotating packed bed with nickel foam packing. *Chem Eng Process Process Intensif* 90:34–40. <https://doi.org/10.1016/J.CEP.2015.02.007>
64. Luo Y, Luo JZ, Chu GW, Zhao ZQ, Arowo M, Chen JF (2017) Investigation of effective interfacial area in a rotating packed bed with structured stainless steel wire mesh packing. *Chem Eng Sci* 170:347–354. <https://doi.org/10.1016/J.CES.2016.10.023>
65. Liu W et al (2019) Mass transfer in a rotating packed bed reactor with a mesh-pin rotor: modeling and experimental studies. *Chem Eng J* 369:600–610. <https://doi.org/10.1016/J.CEJ.2019.03.081>
66. Neumann K, Hunold S, De Beer M, Skiborowski M, Górak A (2018) Mass transfer studies in a pilot scale RPB with different packing diameters. *Ind Eng Chem Res* 57(6):2258–2266. https://doi.org/10.1021/ACS.IECR.7B04186/SUPPL_FILE/IE7B04186_SI_001.PDF
67. Chen YS, Lin FY, Lin CC, Der Tai CY, Liu HS (2006) Packing characteristics for mass transfer in a rotating packed bed. *Ind Eng Chem Res* 45(20):6846–6853. <https://doi.org/10.1021/ie0603991>
68. Sun BC, Wang XM, Chen JM, Chu GW, Chen JF, Shao L (2009) Simultaneous absorption of CO₂ and NH₃ into water in a rotating packed bed. *Ind Eng Chem Res* 48(24):11175–11180. <https://doi.org/10.1021/IE9001316>
69. Chen YS, Lin CC, Liu HS (2005) Mass transfer in a rotating packed bed with viscous Newtonian and non-Newtonian fluids. *Ind Eng Chem Res* 44(4):1043–1051. <https://doi.org/10.1021/IE0499409>
70. L. Sang, Y. Luo, G. W. Chu, B. C. Sun, L. L. Zhang, and J. F. Chen, “A three-zone mass transfer model for a rotating packed bed,” *AIChE J.*, vol. 65, no. 6, p. e16595, Jun. 2019, doi: <https://doi.org/10.1002/AIC.16595>.
71. Lin CC, Kuo YW (2016) Mass transfer performance of rotating packed beds with blade packings in absorption of CO₂ into MEA solution. *Int J Heat Mass Transf* 97:712–718. <https://doi.org/10.1016/J.IJHEATMASSTRANSFER.2016.02.033>
72. Lin CC, Chu CR (2015) Mass transfer performance of rotating packed beds with blade packings in carbon dioxide absorption into sodium hydroxide solution. *Sep Purif Technol* 150:196–203. <https://doi.org/10.1016/J.SEPPUR.2015.06.025>
73. Sheng M et al (2018) Intensification of CO₂ capture using aqueous diethylenetriamine (DETA) solution from simulated flue gas in a rotating packed bed. *Fuel* 234:1518–1527. <https://doi.org/10.1016/J.FUEL.2018.07.136>
74. Luo Y et al (2012) Mass transfer studies in a rotating packed bed with novel rotors: chemisorption of CO₂. *Ind Eng Chem Res* 51(26):9164–9172. <https://doi.org/10.1021/IE300466F>
75. Jiao WZ, Liu YZ, Qi GS (2010) Gas pressure drop and mass transfer characteristics in a cross-flow rotating packed bed with porous plate packing. *Ind Eng Chem Res* 49(8):3732–3740. <https://doi.org/10.1021/IE9009777>
76. Chu GW et al (2014) Absorption of SO₂ with ammonia-based solution in a cocurrent rotating packed bed. *Ind Eng Chem Res* 53(40):15731–15737. https://doi.org/10.1021/IE502519V/SUPPL_FILE/IE502519V_SI_001.PDF
77. Bai S et al (2015) SO₂ removal in a pilot scale rotating packed bed. *Environ Eng Sci* 32(9):806–815. <https://doi.org/10.1089/EES.2014.0412>
78. Chen Y-S, Lin F-Y, Lin C-C, Yi-Der Tai C, Liu H-S (2006) Packing characteristics for mass transfer in a rotating packed bed. <https://doi.org/10.1021/ie0603991>
79. Joel AS, Wang M, Ramshaw C, Oko E (2014) Process analysis of intensified absorber for post-combustion CO₂ capture through modelling and simulation. *Int J Greenh Gas Control* 21:91–100. <https://doi.org/10.1016/j.ijggc.2013.12.005>
80. Dong YN et al (2021) Green and efficient sulfur dioxide removal using hydrogen peroxide in rotating packed bed reactor: Modeling and experimental study. *Chem Eng Sci* 235:116467. <https://doi.org/10.1016/J.CES.2021.116467>
81. Leung DYC, Caramanna G, Maroto-Valer MM (2014) An overview of current status of carbon dioxide capture and storage technologies. *Renew Sustain Energy Rev* 39:426–443
82. Bernhardsen IM, Knuutila HK (2017) A review of potential amine solvents for CO₂ absorption process: absorption capacity, cyclic capacity and pKa. *Int J Greenhouse Gas Control* 61:27–48. <https://doi.org/10.1016/j.ijggc.2017.03.021>
83. Usubharatana P, Tontiwachwuthikul P (2009) Enhancement factor and kinetics of CO₂ capture by MEA-methanol hybrid solvents. *Energy Procedia* 1(1):95–102. <https://doi.org/10.1016/J.EGYPRO.2009.01.015>
84. Gupta M, da Silva EF, Svendsen HF (2022) Modeling differential enthalpy of absorption of CO₂ with piperazine as a function of temperature. *J Phys Chem B* 126(9):1980–1991
85. Jassim MS, Rochelle G, Eimer D, Ramshaw C (2007) Carbon dioxide absorption and desorption in aqueous monoethanolamine solutions in a rotating packed bed. *Ind Eng Chem Res* 46(9):2823–2833
86. Yi F, Zou HK, Chu GW, Shao L, Chen JF (2009) Modeling and experimental studies on absorption of CO₂ by Benfield solution in rotating packed bed. *Chem Eng J* 145(3):377–384. <https://doi.org/10.1016/J.CEJ.2008.08.004>
87. Tu J, Yeoh G-H, Liu C (2018) Introduction. *Computational fluid dynamics*. Elsevier, Amsterdam, pp 1–31
88. Zhang W, Xie P, Li Y, Teng L, Zhu J (2022) 3D CFD simulation of the liquid flow in a rotating packed bed with structured wire mesh packing. *Chem Eng J* 427:130874. <https://doi.org/10.1016/j.cej.2021.130874>
89. Shi X, Xiang Y, Wen LX, Chen JF (2013) CFD analysis of liquid phase flow in a rotating packed bed reactor. *Chem Eng J* 228:1040–1049. <https://doi.org/10.1016/j.cej.2013.05.081>

90. Zhang W, Xie P, Li Y, Teng L, Zhu J (2020) CFD analysis of the hydrodynamic characteristics in a rotating packed bed with multi-nozzles. *Chem Eng Process Process Intensif* 158:108107. <https://doi.org/10.1016/J.CEP.2020.108107>
91. Yang Y et al (2016) CFD modeling of gas-liquid mass transfer process in a rotating packed bed. *Chem Eng J* 294:111–121. <https://doi.org/10.1016/J.CEJ.2016.02.054>
92. Keyvani M (1998) Operating characteristics of rotating beds
93. Yang Y et al (2016) CFD modeling of gas-liquid mass transfer process in a rotating packed bed. *Chem Eng J* 294:111–121. <https://doi.org/10.1016/J.CEJ.2016.02.054>
94. Wang Z, Wu X, Yang T, Wang S, Liu Z, Dan X (2019) Droplet characteristics of rotating packed bed in H₂S absorption: a computational fluid dynamics analysis. *Processes* 7(10):724. <https://doi.org/10.3390/PR7100724>
95. Wojtasik-Malinowska J, Jaskulski M, Jaskulski M (2022) CFD simulation of gas pressure drop in porous packing for rotating packed beds (RPB) CO₂ absorbers. *Environ Sci Pollut Res* 29(47):71857–71870
96. Qammar H, Gładyszewski K, Górak A, Skiborowski M (2019) Towards the development of advanced packing design for distillation in rotating packed beds. *Chem Ing Tech* 91(11):1663–1673. <https://doi.org/10.1002/CITE.201900053>
97. Wojtasik J, Gładyszewski K, Skiborowski M, Górak A, Piątkowski M (2018) Enzyme-enhanced CO₂ absorption process in rotating packed bed. *Chem Pap* 73(4):861–869. <https://doi.org/10.1007/S11696-018-0647-8>
98. Liu Y, Luo Y, Chu GW, Luo JZ, Arowo M, Chen JF (2017) 3D numerical simulation of a rotating packed bed with structured stainless steel wire mesh packing. *Chem Eng Sci* 170:365–377. <https://doi.org/10.1016/j.ces.2017.01.033>
99. Wang C, Perry M, Rochelle GT, Seibert AF (2012) Packing characterization: mass transfer properties. *Energy Procedia* 23:23–32. <https://doi.org/10.1016/j.egypro.2012.06.037>
100. Balzarotti R, Ambrosetti M, Beretta A, Groppi G, Tronconi E (2020) Investigation of packed conductive foams as a novel reactor configuration for methane steam reforming. *Chem Eng J* 391:123494. <https://doi.org/10.1016/J.CEJ.2019.123494>
101. Structured Packing | Amacs Process Towers Internals. <https://www.amacs.com/packing/structured/>. Accessed 28 Jul 2021
102. Guo T-YY, Shi X, Chu G-WW, Xiang Y, Wen L-XX, Chen J-FF (2016) Computational fluid dynamics analysis of the micromixing efficiency in a rotating-packed-bed reactor. *Ind Eng Chem Res* 55(17):4856–4866. <https://doi.org/10.1021/ACS.IECR.6B00213>
103. Guo TY, Cheng KP, Wen LX, Andersson R, Chen JF (2017) Three-dimensional simulation on liquid flow in a rotating packed bed reactor. *Ind Eng Chem Res* 56(28):8169–8179. <https://doi.org/10.1021/ACS.IECR.7B01759>
104. Li H, Yuan Z, Liu Y, Liu H (2019) Characteristics of liquid flow in a countercurrent rotating bed. *Chem Eng Process Process Intensif* 136:72–81. <https://doi.org/10.1016/J.CEP.2018.12.004>
105. Wu W, Luo Y, Chu GW, Liu Y, Zou HK, Chen JF (2018) Gas flow in a multiliquid-inlet rotating packed bed: three-dimensional numerical simulation and internal optimization. *Ind Eng Chem Res* 57(6):2031–2040. <https://doi.org/10.1021/acs.iecr.7b04901>
106. Ouyang Y, Zou HK, Gao XY, Chu GW, Xiang Y, Chen JF (2018) Computational fluid dynamics modeling of viscous liquid flow characteristics and end effect in rotating packed bed. *Chem Eng Process Process Intensif* 123:185–194. <https://doi.org/10.1016/j.cep.2017.09.005>
107. Zhang JP, Liu W, Luo Y, Chu GW, Zou HK, Chen JF (2019) Enhancing liquid droplet breakup by hydrophobic wire mesh: Visual study and application in a rotating packed bed. *Chem Eng Sci*. <https://doi.org/10.1016/J.CES.2019.115180>
108. Bai Y, Zhao Q, Zhang Z, Wang Q, Wang F (2022) A new rotor structural design method of rotating packed bed based on hydrodynamic performance analysis. *Chem Eng Process* 181:109145. <https://doi.org/10.1016/J.CEP.2022.109145>
109. Chen YS, Liu HS (2002) Absorption of VOCs in a rotating packed bed. *Ind Eng Chem Res* 41(6):1583–1588. <https://doi.org/10.1021/IE010752H>
110. Lin CC, Chien KS (2008) Mass-transfer performance of rotating packed beds equipped with blade packings in VOCs absorption into water. *Sep Purif Technol* 63(1):138–144. <https://doi.org/10.1016/J.SEPPUR.2008.04.007>
111. Lu X et al (2019) Modelling of CO₂ absorption in a rotating packed bed using an Eulerian porous media approach. *Chem Eng Sci* 199:302–318. <https://doi.org/10.1016/J.CES.2019.01.029>
112. Lu X, Xie P, Ingham DB, Ma L, Pourkashanian M (2018) A porous media model for CFD simulations of gas-liquid two-phase flow in rotating packed beds. *Chem Eng Sci* 189:123–134. <https://doi.org/10.1016/j.ces.2018.04.074>
113. Kołodziej A, Łojewska J (2009) Experimental and modelling study on flow resistance of wire gauzes. *Chem Eng Process Process Intensif* 48(3):816–822. <https://doi.org/10.1016/j.cep.2008.10.009>
114. Das S, Deen NG, Kuipers JAM (2018) Multiscale modeling of fixed-bed reactors with porous (open-cell foam) non-spherical particles: hydrodynamics. *Chem Eng J* 334:741–759. <https://doi.org/10.1016/J.CEJ.2017.10.047>
115. Alkhalaf A, Specht E (2017) Prediction of cross flow mixing in the structured packed bed through CFD simulation using (FBM and PMM) and validation with experiments. *Eng Appl Comput Fluid Mech* 11(1):1–4
116. Lu X, Xie P, Ingham DB, Ma L, Pourkashanian M (2019) Modelling of CO₂ absorption in a rotating packed bed using an Eulerian porous media approach. *Chem Eng Sci* 199:302–318. <https://doi.org/10.1016/J.CES.2019.01.029>
117. Guerrero E, Muñoz F, Ratkovich N (2017) Comparison between eulerian and vof models for two-phase flow assessment in vertical pipes. *CTyF* 7(1):73–84. <https://doi.org/10.29047/01225383.66>
118. Wu W et al (2020) Liquid flow behavior in a multiliquid-inlet rotating packed bed reactor with three-dimensional printed packing. *Chem Eng J* 386:121537. <https://doi.org/10.1016/J.CEJ.2019.04.117>
119. Khan Z, Bhusare VH, Joshi JB (2017) Comparison of turbulence models for bubble column reactors. *Chem Eng Sci* 164:34–52. <https://doi.org/10.1016/j.ces.2017.01.023>
120. Yang Y et al (2015) 3D CFD modelling and optimization of single-phase flow in rotating packed beds. *Can J Chem Eng* 93(6):1138–1148. <https://doi.org/10.1002/cjce.22183>
121. Llerena-Chavez H, Larachi F (2009) Analysis of flow in rotating packed beds via CFD simulations—dry pressure drop and gas flow maldistribution. *Chem Eng Sci* 64(9):2113–2126. <https://doi.org/10.1016/J.CES.2009.01.019>
122. Sebastia-Saez D, Gu S, Ranganathan P, Papadakis K (2015) Micro-scale CFD modeling of reactive mass transfer in falling liquid films within structured packing materials. *Int J Greenh Gas Control* 33:40–50. <https://doi.org/10.1016/j.ijggc.2014.11.019>
123. Sebastia-Saez D, Gu S, Ranganathan P (2014) Volume of fluid modeling of the reactive mass transfer of CO₂ into aqueous amine solutions in structured packed elements at microscale. *Energy Procedia* 63:1229–1242. <https://doi.org/10.1016/j.egypro.2014.11.133>
124. Gbadago DQ, Oh HT, Oh DH, Lee CH, Oh M (2020) CFD simulation of a packed bed industrial absorber with interbed liquid distributors. *Int J Greenh Gas Control*. <https://doi.org/10.1016/j.ijggc.2020.102983>